Practical concept of arbitrary anisotropy applied in traveltime inversion of simulated P-wave VSP data

Ivan Pšenčík [1], Bohuslav Růžek [1] and Petr Jílek [2]

[1]Institute of Geophysics, Acad. Sci. of Czech Republic, Boční II, 141 31 Praha 4, Czech Republic. E-mail: ip@ig.cas.cz; b.ruzek@ig.cas.cz

[2]BP America Inc., Subsurface Technology Center, 501 WestlakePark Blvd., Houston, TX 77079, USA. E-mail: petr.jilek@bp.com

Summary

We show that it is possible, and often desirable, to accommodate arbitrary P-wave anisotropy in practical seismic data processing, including migration and full waveform inversion. We propose a practical concept of arbitrary P-wave anisotropy, providing a sufficient degree of freedom to explain and reproduce observed anisotropic seismic signatures to a high degree of accuracy. The key to this concept is the proposed P-wave anisotropy parameterization (A-parameters) that, together with the use of the weak-anisotropy approximation, leads to significantly simplified theory. Here as an example, we use a simple and transparent formula relating P-wave traveltimes and 15 P-wave A-parameters. The formula is used in the inversion scheme, which does not require any a priori information about anisotropy symmetry and its orientation. We test applicability of the proposed scheme on a blind inversion of synthetic P-wave traveltimes generated for VSP experiments in homogeneous models. Three models of varying anisotropy are used: tilted orthorhombic and triclinic models of moderate anisotropy ($\sim 10\%$), and orthorhombic model with a horizontal plane of symmetry, of strong anisotropy ($> 25\%$). In all cases, the inversion yields all 15 P-wave A-parameters, which make reconstruction of corresponding phase-velocity surfaces possible with a high degree of accuracy. The inversion scheme is robust with respect to noise and source distribution. Its quality depends on the angular illumination of the medium. The results of the inversion are applicable, for example, in migration or as a starting model for inversion methods, such as full waveform inversion, if a model refinement is desired.

Introduction

One of the main challenges of seismic data processing in oil industry today is estimating velocity-anisotropy models adequate for high-accuracy, high-resolution seismic imaging, interpretation, and characterization of hydrocarbon reservoirs. Transverse isotropy (TI) models, including TI models with tilted axis of symmetry (TTI), have been successfully used in the industry for more than a decade, setting the industry standard (Huang et al., 2008; Rollins et al., 2013; Reta-Tang et al., 2015; Jin et al. 2018). In recent years, orthorhombic (ORT) or tilted-orthorhombic (TOR) models have been gaining increasing attention for a simple reason: high-quality, high-density, multi-azimuth seismic data

Seismic Waves in Complex 3–D Structures, **28** (2018), 9–44 (ISSN 2336–3827, online at http://sw3d.cz)

acquired today support, and often clearly reveal, lower anisotropy symmetry in the subsurface (see, for example, Wu et al., 2013, Mathewson et al., 2015, or Zhou et al, 2015). Embracing opportunities and challenges that such data sets offer, we often have to reach beyond conventional approaches while striving for a step-change in our seismic imaging and characterization capabilities. With that on mind, our intention here is to offer a novel practical approach to arbitrary anisotropy as a cost-effective concept applicable to P-wave data processing that becomes especially useful when anisotropy symmetry of the subsurface is low, tilted, changing, or highly uncertain. (Note that, although not discussed here, the concept is also applicable to S-waves, which will be subject of future studies.)

In conventional anisotropy model building process, we typically start by making an a priori assumption about the anisotropy symmetry (such as TTI or TOR in the case of observable azimuthal variations). The assumption is made out of the necessity to constrain and simplify the process, which is often driven by our existing (limited) processing capabilities and/or associated cost. Next step is to estimate the corresponding orientation of the assumed anisotropy symmetry. It is usually an iterative and elaborate process, especially for TOR media, see, for example, Li et al. (2012) or Zdraveva et al. (2015). It includes an interpretation step, nearly always based on yet another assumption: one symmetry plane is always parallel to bedding (Audebert et al., 2006; Alkhalifah and Sava, 2010; Zdraveva and Cohan, 2011). Such an assumption is plausible in benign shale-sand formations, for example, but it becomes more speculative in areas with pronounced stress regimes (near-salt, faulted zones, tectonic stresses, etc.) or in highly fractured zones with different fracture orientations. Moreover, estimating structural dips has its own practical issues (such as conflicting or highly-variable dips or noise interference). Some alternative approaches thus have been suggested, for example, by Bakulin at al. (2009) or Thanoon et al. (2016). The estimate of anisotropy symmetry and its orientation is thus largely decoupled, and without a direct feedback, from the corresponding anisotropy parameter estimation that typically follows. The inversion becomes strongly non-linear otherwise.

After establishing the anisotropy symmetry and orientation, the anisotropy model estimation further suffers from tradeoffs in between anisotropy and heterogeneity, and tradeoffs among individual anisotropy parameters themselves, largely because we are often attempting to invert for, and even interpret, parameters that are not well-constrained by data acquired during a given experiment. Although separating the effects of heterogeneity and anisotropy is a difficult problem that may never be fully resolved, it is clear that choosing a proper, data-driven parameterization that minimizes the cross-talk among the parameters is critical. However, a lack of analytic insight, especially for anisotropy symmetries lower than TI, usually prevents us from parameterizing anisotropy effectively. Constraining the inversion algorithms that involve anisotropy (such as tomography or FWI) thus quickly becomes difficult. Therefore, in practice we usually further constrain the inversion by inverting separately for anisotropy parameters and a reference velocity (such as the velocity along an assumed symmetry axis) by freezing one and inverting for the other. For example, anisotropy parameters can initially be obtained from previous (time) processing, from extrapolated well information, or is inherited from previous projects in the region. In the model-building flow that follows, anisotropic FWI is often ran to update the velocity while the anisotropy parameters are kept unchanged. Anisotropic tomography may be carried out afterwards with fixed velocity field to reduce residual moveouts along image gathers by adjusting the anisotropy parameters. The process may

iterate. Such velocity and anisotropy parameters freezing makes sense namely because the magnitude difference: inversion is typically more sensitive to the bigger velocity than the much smaller anisotropy parameters. In the end, the reference velocity absorbs most of the heterogeneities, the anisotropy parameter fields typically remain smooth. One can speculate whether such a freezing approach is appropriate or not. However, the bottom line is we usually do not have any better way to carry out (and control) the inversion process that would also be stable and practical. Adopting a full non-linear, production-scale inversion for 21 elastic parameters per grid point as an alternative, resulting in significant theoretical and computational complexities, lacking physical insight, and offering no guarantee to improve the results that justify the cost, seems unlikely.

To be fair, the above-described approaches often do work in practice in the sense that the results improve (Rollins et al., 2013; Mathewson et al., 2015; Reta-Tang et al., 2015). But what if we could do better, exploiting the potential of acquired datasets more thoroughly and with a less of an effort? What if we could remove altogether the assumption of anisotropy type, and the need to estimate the symmetry orientation, so the anisotropy can be arbitrary and as data dictates? Clearly, if the anisotropy symmetry is assumed incorrectly a priori, corresponding seismic images degrade (Vestrum et al., 1999; Kumar et al., 2004; Behera and Tsvankin, 2007). Also, historically, as the data quality improves over time, we often realize that it is impossible to explain some newly-observed data features (as was the case of azimuthally varying image gathers, for example). Such observations eventually lead to reconsidering the assumed anisotropy type and, once again, developing and re-designing imaging and inversion algorithms to accommodate the new anisotropy symmetry (such as TOR most recently). It is conceivable that with increasing data quality, coverage, and data density it may happen again in future. In fact, it is conceivable that, at some point, we may desire to routinely handle arbitrary anisotropy regardless of its symmetry and orientation (also potentially removing troublesome widespread inconsistencies in symmetry-orientation conventions adopted across industry and academia). What follows is our attempt to make a step in this direction.

The purpose of this paper is two-fold. First, we would like to offer a conceptionally different view on seismic anisotropy, removing some major assumptions and inversion issues discussed above: anisotropy is primarily used to provide a sufficient degree of freedom to explain observed seismic data without necessarily interpreting each anisotropy parameter at every processing step. Such an anisotropy, as an effective medium that explains the data, can be estimated in principle and, subsequently, used in seismic imaging. (The interpretation step may follow later if desired.) Such anisotropy concept is realized via implementing an adequate anisotropy parameterization that does not care about a specific anisotropy symmetry, does not suffer from mixing different units, and that merely represents measurable (i.e., constrained by data) combinations of stiffness tensor elements. Second purpose of this paper is to demonstrate the introduced concept on a blind inversion of synthetic P-wave VSP data, generated in a homogeneous medium of arbitrary anisotropy, following the basic idea of blind tests previously introduced and carried out by industry, see Billette and Brandsberg-Dahl (2004), Neep (2008), or Dellinger et al. (2015) for corresponding BP examples. (Blind means that the inversion is carried out separately from the data preparation, by different team, and without a priori knowledge of the true model.) The synthetic data is used as our first step only to maintain full control over the experiment. On the other hand, and as we discuss below, to keep the demonstration

meaningful we make a diligent effort to mimic real-data processing scenario (no inversion crime committed, data contaminated by noise extracted from field VSP data, P-wave arrivals picked using commercial processing software, etc.).

The paper has the following structure. First, we introduce the proposed concept of practical arbitrary anisotropy and its estimation, including the so-called A-parameterization. Then we set up the VSP experiment. In the next section, we present an approximate formula for the square of P-wave ray velocity in terms of 15 P-wave A-parameters used in the inversion. The A-parameters describe P-wave anisotropy of arbitrary strength, symmetry and orientation. The above expression is used in the next section to formulate the inverse problem. Then the data preparation and the experiment configuration are described, followed by the inversion results and their discussion. Last section contains conclusions and future plans. In Appendix A, we describe the used inversion scheme. Appendix B contains definitions of P-wave A-parameters and Appendix C shows revealed matrices of elastic parameters in the Voigt notation of the used models.

Practical approach to arbitrary anisotropy parameterization: the concept

Although there may be various reasons to consider it, bringing arbitrary anisotropy into seismic data processing immediately results in significant practical challenges. We need 21 elastic parameters at every point of the subsurface. The theory becomes significantly more complex, usually lacking any physical insight. The resulting computations become costly. Even if we are willing to take on these challenges, the main problem remains: How do we estimate the 21 elastic parameters from a seismic experiment? There is often no clear understanding of how individual elastic parameters are constrained by data and how they relate to measurable seismic attributes. Setting up effective inversion schemes thus becomes difficult.

In our practical approach we are seeking a set of anisotropy parameters that provides a sufficient (i.e., the least) degree of freedom needed to describe any observed data to a high degree of accuracy. In other words, in this first stage we are not primarily interested in interpretation of the anisotropy parameters, as we typically tend to do in higher symmetry media, as much as we are interested in extracting a measurable, data-constrained medium parameters (in our case, combinations of stiffness tensor elements) that, in turn, can be used to accurately reproduce kinematics (and potentially dynamics) of the observed seismic wavefields. Corresponding wave propagators (used in modeling, migrations, tomography, FWI, etc.) can then be designed utilizing the same parameter set. Such propagators would be "universal" in the sense that they would not be limited to any type and orientation of anisotropy in any given experiment. Importantly, no interpretation in the process of anisotropy recovery is involved. Of course, in principle, the estimated parameters can also be converted into more conventional anisotropic parameters, at least for higher anisotropy symmetries such as TI or orthorhombic (Thomsen, 1986; Tsvankin, 1997), and then interpreted, if desired. Here, however, we argue that for certain important applications such as modeling and migrations (including inversion-migration iterative flows) this is not necessary.

Besides the close relation to measurements, we also require simplicity in the anisotropy description, allowing for analytic insight and resulting in simplified theory and reduced

computational cost. Below we show that this is possible to a large degree. The key is, of course, an adequate parameterization. We use the so-called A-parameters (anisotropy parameters) introduced and discussed by Pšenčík et al., (2018). The A-parameters resulted from a slight modification of originally introduced WA (weak-anisotropy) parameters parameters, see, e.g., Farra et al. (2016) for their detailed discussion and history of their introduction. The modification reflected a more natural relation of A-parameters to P- and S-wave measurements while eliminating some unnecessary internal dependencies remaining among WA parameters. Without any further details, the A-parameters [definition (B1)] represent linear combinations of stiffness tensor elements that control, to the first-order weak-anisotropy approximation, various seismic quantities and attributes (e.g., traveltimes, velocities, polarizations, amplitudes) and hence are measurable and extractable from seismic data experiments in principle, depending on the data coverage.

Although A-parameters are related to the weak-anisotropy concept, the weak-anisotropy assumption is not required. A-parameters are defined to describe anisotropy of any strength, being fully equivalent to stiffness tensor elements. The weak-anisotropy approximation in conjunction with A-parameters, however, plays an important role. The WA and/or A-parameters were used to develop various new anisotropic relations and methods in the past (e.g., Farra and Pšenčík, 2003) that significantly simplify when the weak-anisotropy approximation is employed. Mainly, the P- and S-waves become decoupled, each being described by two separate sets of only 15 (out of 21) P- and S-wave A-parameters in arbitrary anisotropic media. This has important consequences in practice. For instance, many P-wave migration codes today (Kirchhoff, WEM, or RTM), as well as P-wave inversion and modeling codes including tomography and FWI, can be extended to arbitrarily anisotropic media by, in principle, a relatively simple alteration of their kernels (i.e., by merely adding appropriate terms) without generating numerical artifacts due to the coupling of P- and S-wave equations. For example, the non-physical assumption (for solid Earth) of zero S-wave velocity along a symmetry axis (Alkhalifah, 1998), often referred to as "pseudo-acoustic approximation" (Fowler et al., 2010) and often used in industry to make the decoupling possible (Alkhalifah, 2000; Duveneck et al., 2008; Fowler and King, 2011), is not needed/used here even in the case of arbitrary, but weak or even moderate, anisotropy.

Furthermore, although not discussed here, treating S-waves in anisotropic media may become in principle similar to that of P-waves (although there are additional practical challenges with S-wave processing, of course).

Understandably, the weak-anisotropy approximation can be challenged by many. (Core measurements, for example, often indicate strong local anisotropy of in-situ rocks.) However, we suggest that using the weak anisotropy assumption is often justified by making the following arguments. First, perhaps surprisingly, the weak-anisotropy approximation is broadly used in industry already. For example, it can be shown that many of the anisotropic propagators used in production-scale RTM and FWI referred to as "pure acoustic" propagators (as opposed to pseudo-acoustic) are either direct implementations of the weak-anisotropy assumption (Chu et al., 2011; Zhan et al., 2012; Chu et al., 2013) or involve dispersion relations closely related to it that are also comparable in accuracy (Etgen and Brandsberg-Dahl, 2009; Witte et al., 2016; Li and Zhu, 2018). Well documented success of such codes suggests that the weak-anisotropy approximation, in the sense of effective medium, is reasonable. It simply makes difficult things practical. Sec-

ond, over many previous studies using A- (or WA-) parameterization (Farra and Pšenčík, 2003, 2016; Farra et. al., 2016; Farra and Pšenčík (2017), Pšenčík and Farra, 2017; Pšenčík et al., 2018), one can observe that even if the weak-anisotropy approximation is adopted and then violated, sufficiently accurate results are often obtained (in moderately anisotropic media covering anisotropy strengths up to, and even over, 20%). It was this observation that lead us to the suggestion that the A-parameterization can be effective. It offers the least and necessary degree of freedom, and the needed analytic simplicity at the same time, to accurately describe (in the first-order sense) anisotropic properties of seismic wavefields regardless of anisotropy symmetry and orientation. Additionally, we show below that even if recovered values of A-parameters are less accurate (i.e., cases of anisotropy stronger than 20%), the corresponding wave propagation is described accurately in the measured directions of propagation, which is, again, the key information for algorithms like modeling or migration.

We therefore suggest that A-parameterization should be well-suited for practical P- (and S-) wave seismic data processing not only in arbitrarily anisotropic media but also in media with simpler but tilted anisotropy symmetry (TTI, TOR). When tilted, the anisotropy becomes formally arbitrary again although some of the parameters are mutually inter-related. The A-parameterization allows to handle such an arbitrary anisotropy without any need for known symmetry type and orientation, while preserving the simplicity, keeping the cost manageable.

Traveltime inversion of VSP data in media of arbitrary anisotropy

Next, we demonstrate the above-discussed concept by inverting synthetic 3D VSP traveltime data of anisotropy symmetry that is not a priori known. A VSP experiment represents a simpler inversion problem (known depths, reasonable angular illumination around the borehole), which is the reason why we start with this configuration. In our minds, this is only the first step, the first proof of the concept. Inversions of more realistic/real VSP data, reflection tomography, etc., should follow in future.

There were various attempts of direct-wave traveltime inversion for anisotropic medium properties made in the past. Let us mention, for example, Hirahara and Ishikawa (1984), Chapman and Pratt and (1992), Pratt and Chapman (1992), Jech and Pšenčík (1992), Watanabe et al. (1996), Wu and Lees (1999), Mensch and Farra (2002), Zhou et al. (2008). In these and many other papers, the authors faced problems of insufficient illumination of the medium, problems with the determination of complete sets of medium parameters, and problems with distinguishing the effects of anisotropy from the effects of heterogeneity. To simplify their inversions, the authors simplified their anisotropic models. They considered, for example, higher-symmetry anisotropic media, 2D models, or they used the so-called factorized anisotropy concept (Červený, 1989), which reduced the number of required model parameters considerably. For more recent attempts, see, e.g., Bai et al., (2016), including their references. Here we demonstrate how the use of A-parameterization discussed above results in a simplified practical inversion without limiting assumptions about the anisotropy symmetry. Of course, we could also assume the symmetry and its orientation known, as in conventional approaches, by specifying a priori certain A-parameters. However, the point here is the opposite: to show that certain estimated A-parameters effectively vanish, indicating higher anisotropy symmetry whose

symmetry elements (symmetry planes/axes) coincide with the coordinate planes/axes. In our approach, we deduce the anisotropy type and orientation from the inversion results, not the other way around.

Before we approach the VSP inversion in 3D inhomogeneous media as the next step, we wish to understand how the inversion performs in homogeneous arbitrary anisotropic media. In practice, this would be the case, for example, of rock-physics laboratory measurements and their interpretations, see, e.g., Jech (1991), Arts (1993), Vestrum (1994), Mahmoudian et al. (2014) or Svitek et al. (2014). For the use of WA parameters, see Růžek and Pšenčík (2016), for the use of A-parameters, see Pšenčík et al. (2018). In this paper, however, we want to use a configuration more relevant to seismic exploration. In contrast to laboratory studies of anisotropic samples, which allow complete sample illumination from all directions, we therefore consider a VSP configuration, which allows for partial illumination only. In the following, we concentrate on inversion of P-wave traveltimes only.

Since we consider a homogeneous medium, there is no need for tracing rays, which would be otherwise required in the forward-modeling part of the inversion. The rays are straight lines connecting sources and receivers with traveltimes along them controlled by the ray (group) velocity vectors. To find the ray-velocity vector corresponding to a given source-receiver direction is, however, not a trivial task. In general, it requires a two- point ray-tracing-like procedure. In order to avoid this complication in our and future experiments, we use, once again, the weak-anisotropy approximation applied to the ray velocity. Instead of using its exact formula, we use its first-order weak-anisotropy approximation, see, for example, Farra and Pšenčík (2016) or Farra et al. (2016). The resulting approximate formula used here is based on a seemingly severe assumption that, in the first-order weak-anisotropy approximation, the ray-velocity vector can be approximated by the phase-velocity vector (both in its magnitude and direction). It is worthy to point out that this approximation is the least accurate out of the three approximations introduced by Farra and Pšenčík (2016). Nevertheless, its maximum relative errors vary between 2% and 3% in realistic anisotropic models.

An obvious concern can rise that such a broad use of the weak-anisotropy approximation throughout the inversion, which essentially means a linearization in A-parameters, inevitably results in a significant loss of accuracy. We have investigated the accuracy aspects before, see Růžek and Pšenčík (2016), and we continue with this investigation in the numerical experiments below. For now, let us just re-emphasize the main practical benefits of this approach:

a) we use explicit, relatively simple and transparent approximate formulae for the ray velocity (Farra and Pšenčík, 2016), depending directly on the source-receiver (ray) direction (which in our special homogeneous case also removes the necessity to perform the two-point ray-tracing-like procedure mentioned above);

b) it becomes possible to arrange the equations relating the traveltimes to parameters of the medium into the system of linear equations invertible for A-parameters;

c) the number of medium parameters to invert for reduces significantly; instead of 21 elastic parameters, we need only 15 P-wave A-parameters specifying most general anisotropy (Farra et al., 2016; Pšenčík et al., 2018).

Approximate, closed-form traveltime formulae in A-parameterization

Traveltime t is related to the parameters a_{ijkl} (density-normalized stiffness tensor for arbitrary anisotropy) through the ray (group) velocity $v = v(\mathbf{N}, a_{ijkl})$, where $\mathbf{N}$ denotes the *ray vector*, a unit vector parallel to the ray-velocity vector. In the case of a homogeneous medium, this vector coincides with the direction from the source to the receiver. Adopting the weak-anisotropy approximation discussed above, it is possible to express the P-wave ray velocity (or its various powers) in terms of only 15 P-wave A-parameters in media of arbitrary anisotropy, see equation (B1) in Appendix B. (Although not discussed here, there is an analogous set of 15 S-wave A-parameters describing S-wave quantities, see Pšenčík et al., 2018.)

In the inversion here, we test the traveltime approximation based on the squared ray velocity v^2, which is related linearly to the A-parameters. The use of v^2 is especially useful in homogeneous (or nearly homogeneous) media, in which we can work directly with velocity rather than traveltimes. Note that in their inversion, Růžek and Pšenčík (2016) tested also the traveltime approximation based on the ray slowness (v^{-1}) applicable in inhomogeneous media, in which case traveltimes themselves are related linearly to A-parameters. This makes the propagation of traveltime errors to A-parameters also linear, hence simple to estimate (model covariance matrix $\mathbf{C}_m$ is just linearly transformed data covariance matrix $\mathbf{C}_d$, see Appendix A).

The expression for v^2 in terms of the A-parameters has the following form:

$$\begin{aligned} v^2(\mathbf{N}) = \alpha^2[1 + 2(\epsilon_x N_1^2 + \epsilon_y N_2^2 + \epsilon_z N_3^2 + \eta_x N_2^2 N_3^2 + \eta_y N_1^2 N_3^2 + \eta_z N_1^2 N_2^2) \\ +4(\chi_x N_2 N_3 + \chi_y N_1 N_3 + \chi_z N_1 N_2 - \xi_{24} N_2^3 N_3 - \xi_{34} N_2 N_3^3 - \xi_{15} N_1^3 N_3 \\ -\xi_{35} N_1 N_3^3 - \xi_{16} N_1^3 N_2 - \xi_{26} N_1 N_2^3)] = r^2/t^2 \ , \end{aligned} \tag{1}$$

see Pšenčík et al. (2018). The expression above follows from the formulae for v^2 expressed in terms of WA parameters by Pšenčík and Gajewski (1998), Farra and Pšenčík (2003).

In equation (1), t is the traveltime and r denotes the corresponding source-receiver distance (in inhomogeneous media computed by means of ray-tracing). The 15 P-wave A-parameters (B1) are weighted by various combinations of the components N_i of the ray vector $\mathbf{N} \equiv (N_1, N_2, N_3)^T$. Note that, in equation (1), the relation between v^2 and A-parameters is linear but the relation between the traveltime t and A-parameters is non-linear. The quantity α in equation (1) has the dimension of velocity and can be understood as a P-wave velocity of a reference isotropic medium with respect to which the A-parameters (B1) are defined. Note that A-parameters depend on the choice of α, but the expression for v^2 does not, although α formally appears in equation (1).

In definitions (B1), the reference velocity α can be chosen arbitrarily but it is desirable that the resulting A-parameters are small, i.e., less than unity. It can be chosen such that one of the P-wave A-parameters equals zero. For example, choosing α as the vertical P-wave phase velocity leads to $\epsilon_z = 0$. This option is equivalent to the parameterization used by Thomsen (1986) in VTI media, in which case the A-parameters reduce to linearized Thomsen parameters. Alternatively, α can be chosen such that the norm of A-parameters is minimized, which leads to the so-called isotropic replacement medium, IRM, see, e.g. Fedorov (1968), Mensch and Rasolofosaon (1997) or Pšenčík and Gajewski

(1998). From practical inversion standpoint, the reference velocity α can be also adopted from an isotropic inversion that is often carried out before anisotropy is considered. In any case, in terms of inversion, α is always a known (chosen) parameter and the corresponding A-parameters are to be estimated.

Equation (1) is approximate. However, in contrast to the corresponding exact equations used for similar inversion studies in homogeneous anisotropic media by, e.g., Jech (1991), Arts (1993), Vestrum (1994) or Mahmoudian et al. (2014), equation (1) provides a clear physical insight into the dependencies of the velocity on the medium parameters. Sensitivity of the inversion to A-parameters (in the first-order, weak-anisotropy approximation sense) thus becomes straightforward to evaluate. The fact that each of the 15 P-wave A-parameters has a different directional dependence in equation (1) indicates that A-parameters can be determined from measurements in principle, provided sufficient angular illumination of the medium. It is immediately obvious that a limited angular illumination will lead to recovery of only a subset of A-parameters. For example, the use of waves propagating in a prevailingly vertical direction gives a chance to recover the A-parameters ϵ_z, ξ_{34} and ξ_{35} while the use of waves propagating in prevailingly horizontal directions will lead to the recovery of ϵ_x, ϵ_y, ξ_{15}, ξ_{16}, ξ_{24} and ξ_{26}. It can be shown (Pšenčík and Gajewski, 1998) that in order to recover all 15 A-parameters, at least 5 different acquisition profiles are necessary. On the other hand, if only a limited subset of A-parameters can be recovered from a given experiment, that should be, in theory, the only subset needed to kinematically describe and reproduce (to the first order) the wave propagation captured by that experiment.

Finally, we would like to point out two consequences of equation (1) important for inversion that are generally valid (not limited to the VSP experiment). First, as the velocity α is known and the ray-velocity (1) is thus solely controlled by small dimensionless A-parameters of comparable magnitudes, the inversion does not suffer from unbalanced sensitivity to various medium parameters due to mixing different units and different orders of magnitude. Second, the estimated A-parameters absorb the effects of both heterogeneity and anisotropy naturally, unlike in conventional inversion flows where the heterogeneity is usually "forced" by design to be mostly captured in the velocity field, and the anisotropy parameters are usually "forced" to remain relatively invariable. It is yet to be seen if the practical inversion for A-parameters in heterogeneous media needs to be additionally constrained in a similar fashion. In theory, that should not be necessary.

Without further constraints, the inversion is naturally balanced and constrained only by directional and spatial data coverage for a given experiment. In turn, the estimated A-parameters, as effective medium parameters, should offer the needed degree of freedom to explain first-order data features measured. Consequently, the estimated A-parameters should be well-suited to sufficiently reproduce, to the first order, the wave propagation captured by the experiment when used in corresponding propagators (such as those used in modeling, Kirchhoff or WE migrations, and FWI). Such modeling or migration codes are not exact, of course, but they become practical, in alignment with the arbitrary anisotropy concept (or the "pure acoustic approximation" concept) discussed.

For further analysis of equation (1), see Farra and Pšenčík (2003), including provided references.

Inversion scheme

Equation (1) for N source-receiver pairs can be arranged in the form of a system of N linear equations to determine 15 unknown P-wave A-parameters from N observed traveltimes t_i corresponding to N source-receiver distances $r_i, i = 1, 2, .., N$. Its matrix form reads:

$$\mathbf{Gm} = \mathbf{d} \ . \tag{2}$$

Here, $\mathbf{G}$ represents an $N \times M$ forward operator matrix, where N is the number of observations and M is the number of sought A-parameters, in our case $M = 15$ (general anisotropy). The rows of matrix $\mathbf{G}$ have the form (A2), see Appendix A. Each row in matrix $\mathbf{G}$ corresponds to one particular source-receiver pair.

Symbol $\mathbf{m}$ in equation (2) denotes the vector of model parameters to be determined. In our case, it consists of 15 P-wave A-parameters, see equation (A4). Vector $\mathbf{d}$ in equation (2) contains known quantities, in our case observed traveltimes t_i and source-receiver distances r_i. Vector $\mathbf{d}$ also contains the known reference velocity α used in the definition of A-parameters (B1). For the explicit form of the vector $\mathbf{d}$ corresponding to the system of equations (1), see equation (A5).

System of equations (2) is solved by means of pseudoinverse described in Appendix A, see equations (A6)-(A10).

VSP experiment configuration

We consider a Cartesian coordinate system x_i, with the x_3-axis vertical, positive downwards. The x_1 - and x_2-axes are horizontal, chosen such that the coordinate system is right-handed. The experiment consists of a vertical borehole located at $x_1 = x_2 = 0$ m with receivers situated along the borehole in five different depth levels: 4000 m, 4250 m, 4500 m, 4750 m, and 5000 m (with one exception of receivers starting at the depth of 1000 m, see below). In all experiments, 150 randomly selected sources are distributed around the borehole on the surface $x_3 = 0$ m, covering offsets up to 6000 m from the wellhead see Figure 1. This configuration involves ray directions up to $\sim 55^\circ$ from vertical, which means that the coverage/representation of large propagation angles is relatively poor. As it is shown later, the omission of rays oriented prevailingly horizontally affects the results of the inversion. In experiments similar to the above specification, Růžek and Pšenčík (2016) showed that such a random, full-azimuth source coverage produces better results compared to a more regular configuration when the same number of sources are regularly distributed along five azimuth profiles (the minimum number of profiles needed to recover all A-parameters).

With the above configuration, we have 750 data points (observations) at our disposal (i.e., $N = 750$), to be used in the inversion based on equation (1).

Data preparation: the blind test

In the past, BP carried out several well-documented blind inversion tests engaging industry and academia to evaluate important model-building tools (Billette et al., 2005; Neep, 2008; Dellinger et al., 2015). Those tests proved to be effective in obtaining more

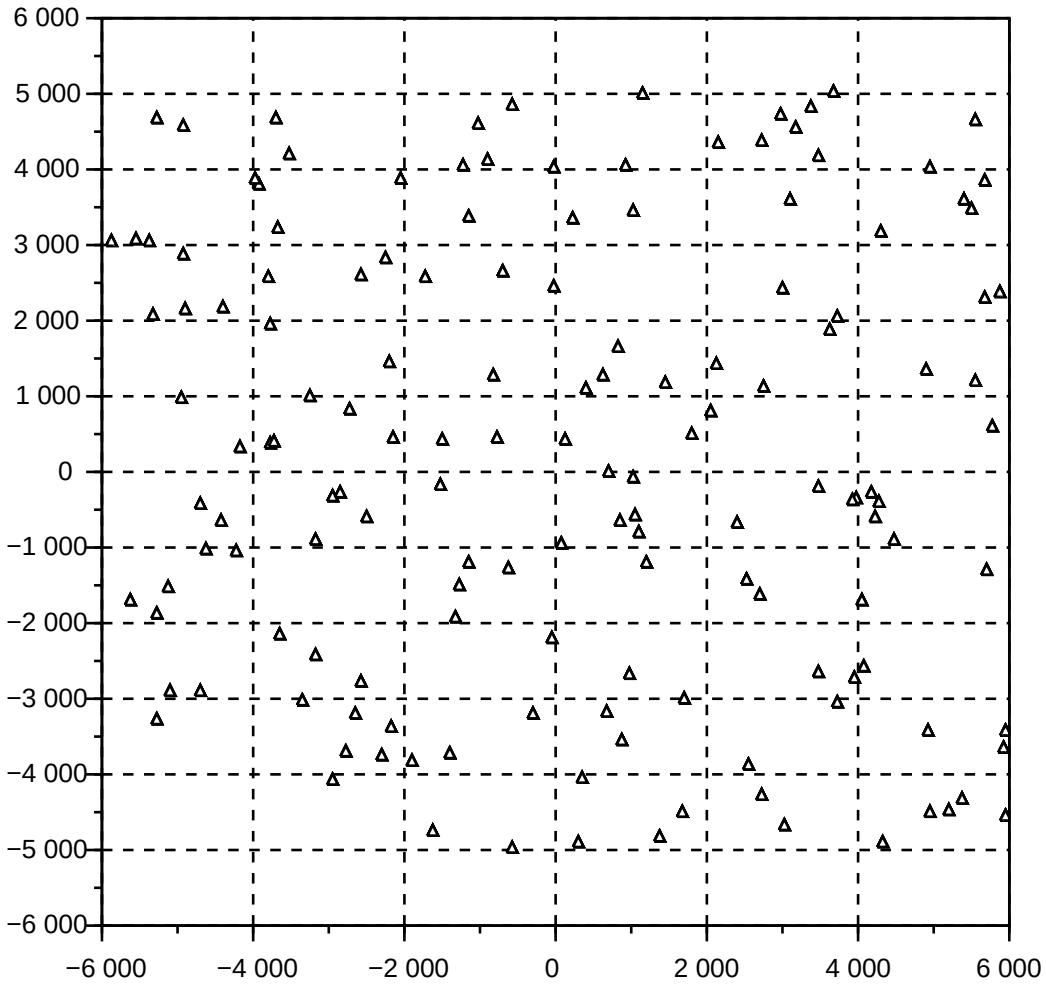

Figure 1: The distribution of 150 randomly selected surface sources around the wellhead ($x_1 = x_2 = 0$ m) used for the inversion.

objective view of accuracy and robustness of the technology being evaluated at the time. In the same spirit, and to mitigate some simplifying assumptions for the sake of objectivity, we decided for a similar approach here. The VSP data was prepared independently by BP (Complex Imaging team, Houston) and then passed to the group at the Institute of Geophysics of Academy of Sciences in Prague for inversion. No a priori information about the model was provided with the data. The only shared information was the VSP configuration (see above), and the agreed fact that the model was homogeneous.

For the inversion tests that follow, three data sets were generated for three anisotropic models labeled as M1, M2, and M3. The models were inspired by real-data examples, representing different anisotropy symmetries of different anisotropy strengths. They are revealed with the estimated results below.

Although the models were always homogeneous, we made a deliberate attempt to

make the inversion as realistic as otherwise possible, adhering to realistic data processing scenario as follows:

a) For each model, BP *elastic* finite difference (FD) modeling was used to generate synthetic VSP data. The data was generated with 4 ms sampling rate on a dense spatial 25 m $\times$ 25 m grid along the surface $x_3 = 0$ m, later decimated according to the configuration described above.

b) The resulting synthetic seismograms were then contaminated by *real* noise extracted from *field* VSP data acquired in Gulf of Mexico (generally uncorrelated background noise).

c) Then, the traveltimes were picked using *standard first-break picking* software, i.e, by techniques commonly used in production-scale data processing. More specifically, an automatic, threshold-based first-break picker was used in combination with correlation of the signal with extracted wavelet to improve the signal onset time estimate.

The resulting traveltimes, as an input to the inversion, thus suffered from realistic non-Gaussian errors, including recorded outliers, different receiver sensitivities/coupling, and natural and cultural noise. They also suffered from some common issues of practical traveltime picking such as errors due to interfering signals, difficulties to set optimal thresholds for automatic traveltime picker due to time-variable (and sometimes poor) S/N, and errors due to imperfect wavelet estimates. Due to adopted model simplifications, traveltime picking was not affected by other coherent noise such as ground roll, multiples, or conversions.

Inversion tests

Model M1

We start with the inversion of traveltimes for model labeled M1. The corresponding traveltimes were generated independently from inversion as described above. Figure 2 shows cross-sections of the synthetic VSP receiver gather at $x_2 = 0$ m (the plane containing the borehole) contaminated by real VSP noise for two borehole receivers at 4000 m and 4750 m, respectively. The P- and both S-wave arrivals are clearly visible through the noise. As in real data, the character of noise varies from receiver to receiver due to different receiver coupling and possibly different instrumental responses. The level of noise contamination was matched to the S/N of the field VSP data, from which the noise was extracted. The data could be considered good-quality. Later we examine the effect of noise by increasing the noise level 2.5 times compared to that in Figure 2, see the discussion of model M2 below.

It is apparent from Figure 2 that the observed arrivals of P- and both S-waves are not exactly symmetric, indicating lower (or tilted) anisotropy symmetry. However, after the data decimation (i.e., a random selection of 150 shot points to be used in the inversion), the azimuthal variation of the P-wave traveltimes is much less obvious to a naked eye. As an example, the picked traveltimes plotted against the distance (hypocentral distance)

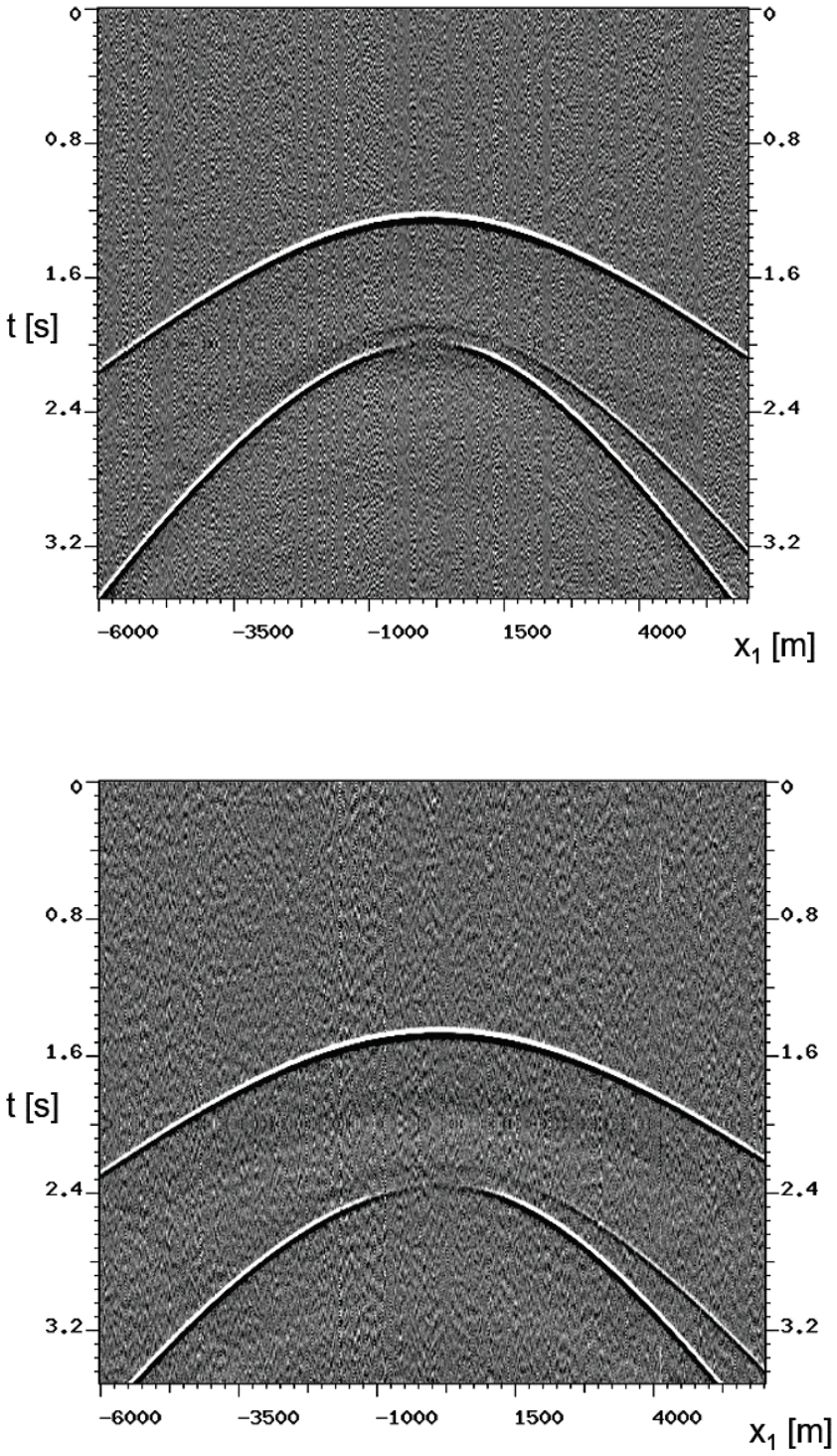

Figure 2: Cross-sections (planes $x_2 = 0$ m) of VSP receiver gather generated for model M1 by elastic FD modeling and contaminated by real VSP noise for borehole receivers at depths $x_3 = 4000$ m (top) and $x_3 = 4750$ m (bottom). Due to anisotropy, the traveltimes are non-symmetric. Notice a few outliers and different noise character between the sections.

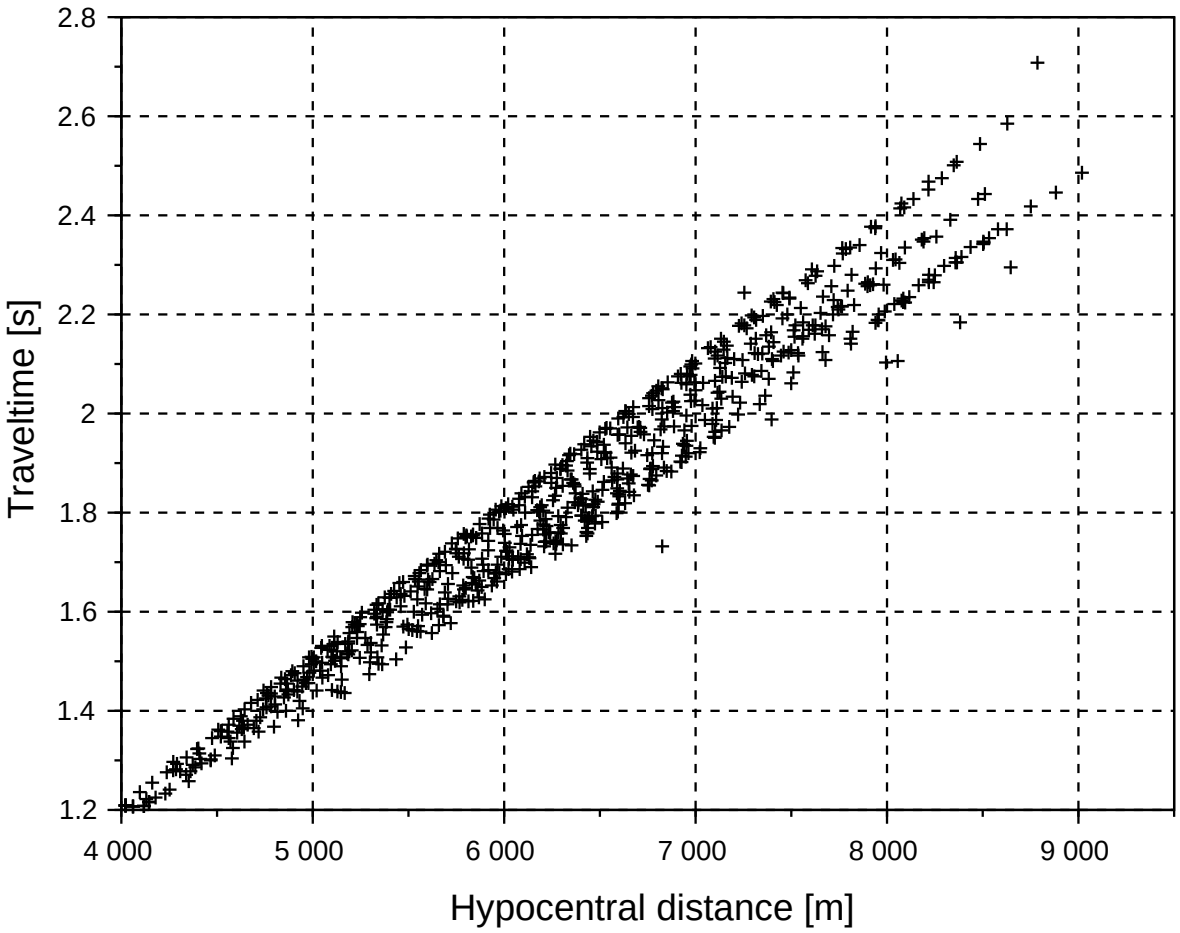

Figure 3: The picked traveltimes plotted against the hypocentral distance of all borehole receivers from surface shots. The picking errors generally increase with the hypocentral distance.

for all five receivers, are shown in Figure 3. The errors of picked traveltimes increase with the hypocentral distance. The actual errors are not necessarily Gaussian.

The blind inversion for 15 P-wave A-parameters was carried out as described above without any assumption about anisotropy symmetry. The results of the inversion are summarized in Figure 4, which shows estimated A-parameters (squares) with corresponding 3-σ errors (error bars in plots correspond to 3-σ error level in order to make them clearly visible). For σ see equation (A10) in Appendix A. The errors indicated by error bars do not account for non-Gaussian errors in data (such as a likely bias in picked traveltimes) and the non-Gaussian errors of the method due to weak-anisotropy approximation. Therefore, they should not be understood as comprehensive error estimates in absolute sense.

Error bars in Figure 4 suggest that most A-parameters should be well-recovered, with the best estimates obtained for ϵ_z, χ_x, χ_y, ξ_{24}, ξ_{34}, ξ_{15} and ξ_{35}. There is, however, a great uncertainty in the determination of parameters η_x, η_y, η_z, ξ_{16} and ξ_{26}. The η and ξ para-

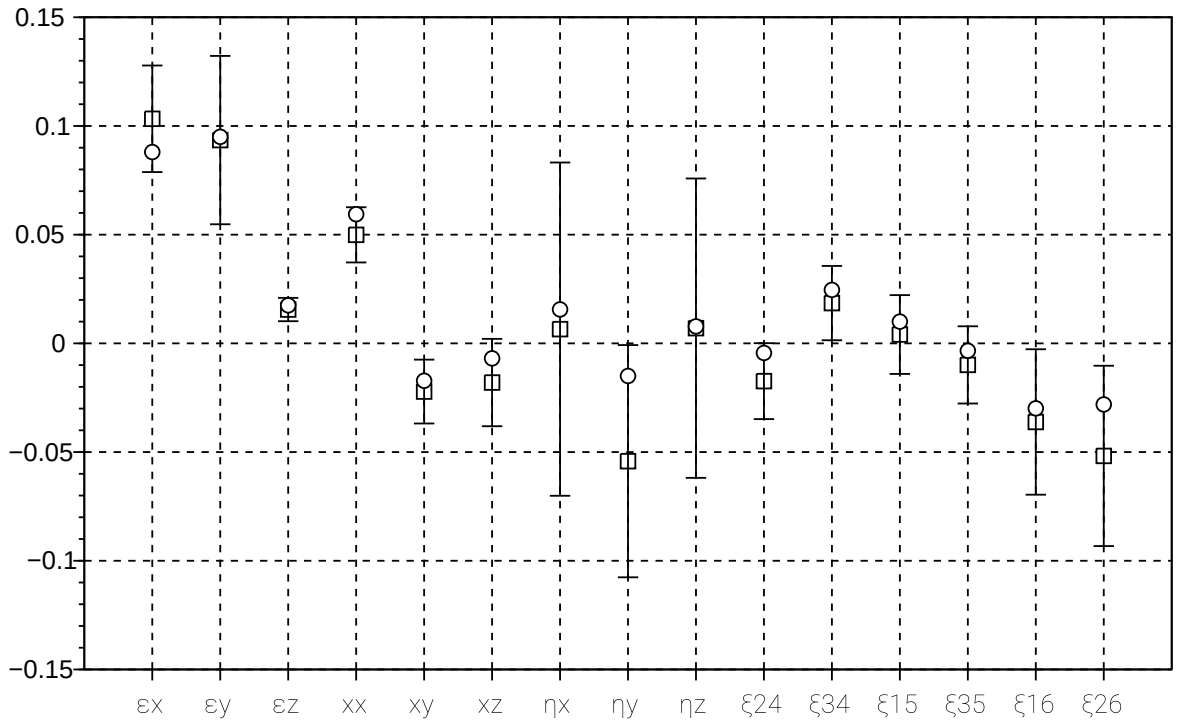

Figure 4: Results of the inversion of traveltime data generated in the model M1 with realistic noise added to 5 receivers distributed regularly between depths of 4 and 5 km. True (circles) and estimated (squares) A-parameters. Demarcated lines: error bars. Reference velocity used: $\alpha = 3.3$ km/s.

meters affect not only P-, but also S-wave propagation. Thus, adding S-waves, which we do not use in this study, could reduce the uncertainty in the determination of η and both ξ parameters (although probably not significantly, see Pšenčík et al., 2018). Likely, the main reason for poor estimates of η and ξ_{16} and ξ_{26} parameters is indicated by the model covariance matrix (Figure 5), showing an obvious correlation of all η parameters with ϵ_x and ϵ_y, and ξ_{16} and ξ_{26} with χ_z parameter (note that ϵ_x, ϵ_y and χ_z are also predicted with a greater uncertainty). This is a clear sign of insufficient data coverage. The lack of certain propagation directions disallows for a complete separation of η and ξ_{16} or ξ_{26} parameters during the inversion. In our next example below (Model M2) we show that the missing propagation directions are the near-horizontal directions. Numerical values of estimated A-parameters are shown in Table 1.

Note that A-parameters from Figure 4 and Table 1 are estimated for a priori chosen background velocity $\alpha = 3.3$ km/s. With the background velocity known, we can further calculate certain medium stiffness tensor elements and their combinations, if desired, using definitions (B1). For example, from ϵ_x, ϵ_y, ϵ_z we can directly estimate vertical and horizontal phase velocities as $V_1 = \sqrt{A_{11}}$, $V_2 = \sqrt{A_{22}}$ and $V_3 = \sqrt{A_{33}}$, respectively. Of course, for a different choice of the background velocity α, the A-parameters would be

Model M1 A parameters	ϵ_x η_z	ϵ_y ξ_{24}	ϵ_z ξ_{34}	χ_x ξ_{15}	χ_y ξ_{35}	χ_z ξ_{16}	η_x ξ_{26}	η_y
true	0.0880 0.0078	0.0950 -0.0044	0.0175 0.0246	0.0594 0.0100	-0.0172 -0.0034	-0.0069 -0.0299	0.0156 -0.0281	-0.0150
estimated	0.1033 0.0070	0.0935 -0.0174	0.0156 0.0185	0.0499 0.0041	-0.0222 -0.0099	-0.0180 -0.0362	0.0065 -0.0518	-0.0542

Table 1: 15 true and estimated P-wave A-parameters of the model M1. P-wave reference velocity chosen $\alpha = 3.3$ km/s.

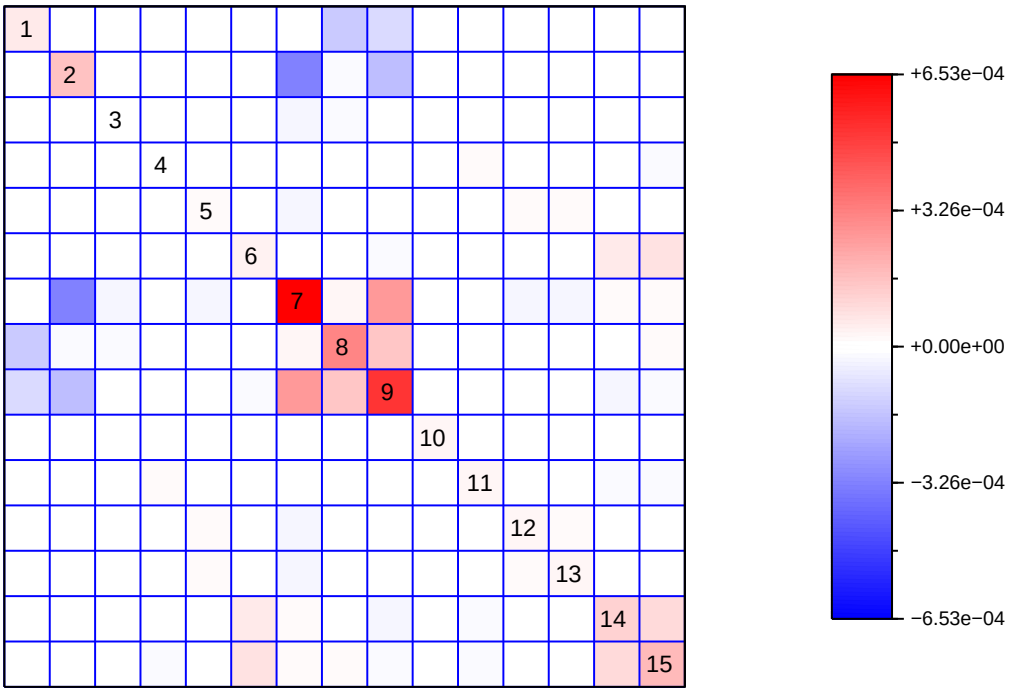

Figure 5: Model covariance matrix related to the inversion of traveltime data generated in the model M1 with realistic noise added to 5 receivers distributed regularly between depths of 4 and 5 km. Diagonal elements indicate the variation of A-parameters. Off-diagonal elements indicate correlation between A-parameters. A-parameters are ordered as in Figure 4 or Table 1.

estimated with different magnitudes. The estimates of the actual medium stiffness tensor elements $A_{\alpha\beta}$, however, would remain the same.

A simple interpretation of the results from Figure 4 confirms that, indeed, model M1 is not isotropic, which would be indicated by all A-parameters being (close-to) zero with the exception of generally non-zero $\epsilon_x = \epsilon_y = \epsilon_z$. The model is not VTI, HTI or ORT (with symmetry planes coinciding with coordinate planes) either, in which cases all the parameters χ_x, χ_y, χ_z, and ξ_{24}, ξ_{34}, ξ_{15}, ξ_{35}, ξ_{16} and ξ_{26} would also be (close-to) zero. The estimated anisotropy of Model M1 can be further interpreted as weak-to-moderate

in strength. (Anisotropy strength can, approximately, be inferred from the values of ϵ_x and ϵ_y with the reference velocity α chosen as the vertical velocity, resulting in $\epsilon_z = 0$; similarly to conventional ϵ-type parameters defined for VTI or orthorhombic media.)

Left plot in Figure 6 shows phase-velocity surface calculated from the estimated A-parameters from Figure 4 (Table 1) using equation (1). By visual inspection of this surface we infer that the model has a pronounced axis of symmetry that passes through the point of, approximately, 20°E and 50°N. We thus finally interpret model M1 as likely to be of either TTI or TOR symmetry. If desired, we could interpret further by making the above-mentioned axis vertical and then rotating the surface around it, examining its rotational symmetry in a greater detail. However, the point here is that such an interpretation of anisotropy symmetry is not necessary (similarly, it is not necessary to know all $A_{\alpha\beta}$) in order to reproduce the velocity function [using equation (1)]. Finally, note that for a different choice of the background velocity α, the phase-velocity surface in the left plot of Figure 6 would remain exactly the same.

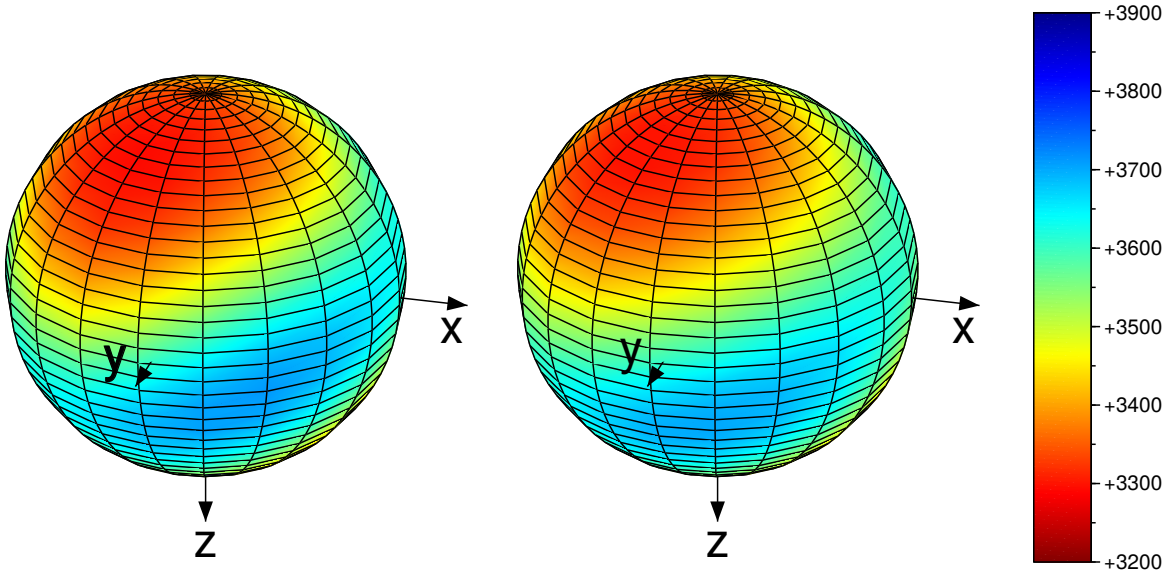

Figure 6: P-wave velocity surfaces calculated from equation (1) for model M1 for 5 receivers distributed regularly between depths of 4 and 5 km. A-parameters estimated from traveltime data (left), true A-parameters (right) used in equation (1).

Model M1 revealed (post-inversion)

Model M1 is, indeed, a model of orthorhombic symmetry, 3D rotated (TOR) as follows: counterclockwise 220° rotation around the x_3-axis, followed by counterclockwise 30° rotation around the new x_1-axis, followed by 150° rotation around the new x_3-axis. The model is inspired by orthorhombic models produced from real data sets over parts of Gulf of Mexico. The anisotropy of the model is moderate ($\sim$ 10%). To evaluate the accuracy of the inversion results, the values of true A-parameters are calculated and added, as open circles, to Figure 4. Their corresponding (true) numerical values can be found in Table 1. (Also, see Appendix C for the matrix of elastic parameters in Voigt notation, before rotation (C1) and after it (C2), used for the FD modeling.) Comparison of estimated and

true A-parameters shows that most of the A-parameters are successfully recovered with numerical accuracy more than acceptable by industry standards. The occurrence of less accurate estimates of η_y, and ξ_{26} is correctly predicted. As discussed above, the real error is more complex than its Gaussian estimate, also including biases in traveltime picking and biases due to approximate theory.

One of the most interesting results of the inversion comes from the comparison of velocity surfaces computed from estimated (left) and true (right) A-parameters in Figure 6. Despite recovery of some of the A-parameters with relatively large errors, the phase-velocity surface based on the recovered parameters reproduces the true phase-velocity surface remarkably well. The velocity formula (1) thus seems to be fairly robust, effectively smoothing out the misfits of individual A-parameters to a large degree. This means that the velocity function, which is the essential quantity for modeling, migration, or FWI, can be reconstructed with a high degree of accuracy, ensuring a proper performance of such algorithms. Such a velocity can be reconstructed without a priori knowledge of anisotropy symmetry and orientation, and even if some A-parameters themselves are not recovered very well. This is probably the most important practical result of the inversion of model M1. We further refine this result in the next inversion example.

Model M2

After a successful blind inversion of model M1, learning basic characteristics, pros, and cons of the inversion, the inversion was put to another test using model M2. The model M2 was prepared, and the noise-contaminated data is (blindly) inverted, in the same manner as in the case of M1 above.

Estimated A-parameters for model M2 are shown as squares in Figure 7, in analogy to Figure 4. Comparing the two results one can see that the distribution of estimated A-parameters in Figure 7 is different from that in Figure 4, indicating that the anisotropy symmetry and orientation are different from that in M1. The anisotropy strength is, again, interpreted as moderate. The error bars in Figure 7 are qualitatively similar to those in Figure 4, which is expected as the source-receiver VSP configuration was the same in both cases. The 3-σ errors in Figure 7 are slightly bigger (note the difference in vertical axes of Figures 4 and 7), indicating higher uncertainties in picked traveltimes and thus estimated A-parameters. (We do not present the corresponding covariance matrix here since it has nearly identical character to that shown in Figure 5.) Note, again, high uncertainties in parameters η_x, η_y, η_z, ξ_{16} and ξ_{26}. Reasons for increased uncertainties of these parameters were discussed during M1 inversion (i.e., limited data angular coverage). Numerical values of estimated A-parameters can be found in Table 2.

Model M2	ϵ_x	ϵ_y	ϵ_z	χ_x	χ_y	χ_z	η_x	η_y
A parameters	η_z	ξ_{24}	ξ_{34}	ξ_{15}	ξ_{35}	ξ_{16}	ξ_{26}	
true	-0.0419	0.0963	-0.0218	-0.1401	-0.0532	0.0088	0.0091	0.2328
	-0.0554	-0.1665	-0.0430	0.0134	-0.0731	-0.0351	0.0499	
estimated	-0.0329	0.0428	-0.0311	-0.1079	-0.0528	-0.0146	0.1009	0.1958
	0.0640	-0.1106	-0.0158	0.0146	-0.0774	-0.0913	0.0007	

Table 2: 15 true and estimated P-wave A-parameters of the model M2. P-wave reference velocity chosen $\alpha = 4.65$ km/s.

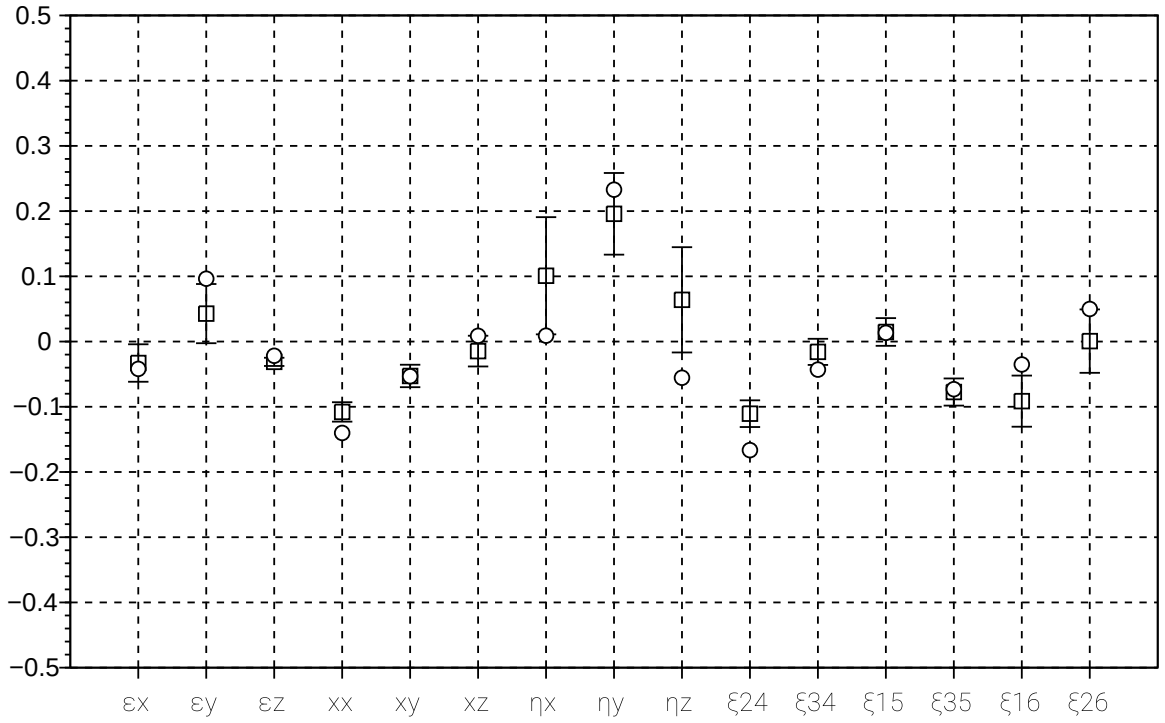

Figure 7: Results of the inversion of traveltime data generated in the model M2 with realistic noise added to 5 receivers distributed regularly between depths of 4 and 5 km. True (circles) and estimated (squares) A-parameters. Demarcated lines: error bars. Reference velocity used: $\alpha = 4.65$ km/s.

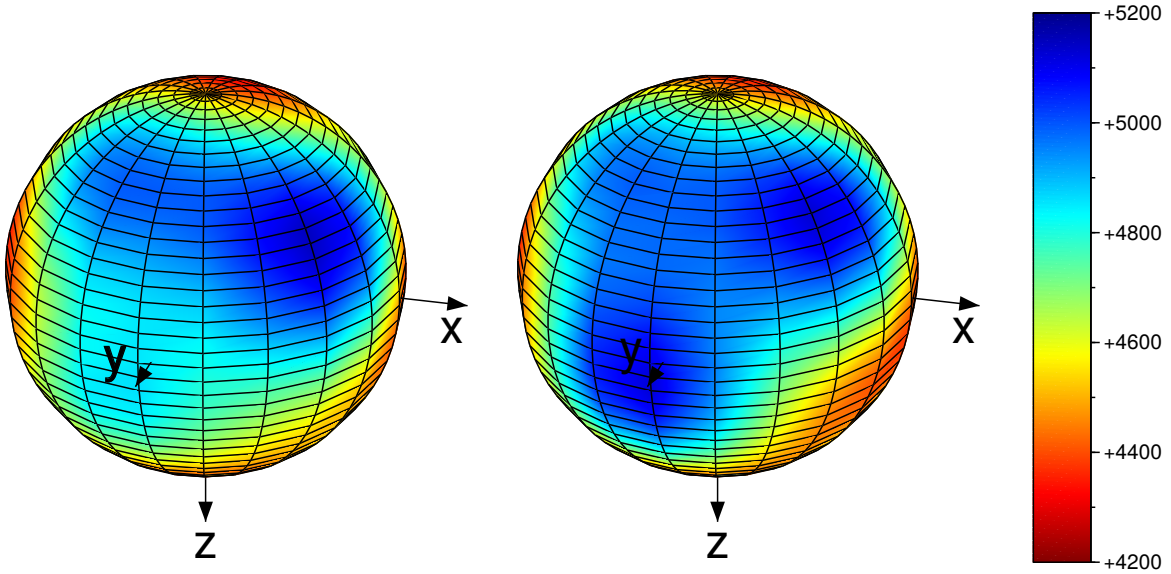

Figure 8: P-wave velocity surfaces calculated from equation (1) for model M2 for 5 receivers distributed regularly between depths of 4 and 5 km. A-parameters estimated from traveltime data and shown in Figure 7 (left), true A-parameters (right) used in equation (1).

The phase-velocity surface in the left plot of Figure 8 computed from the estimated A-parameters in Figure 7 (Table 2) shows strong angular variations of phase velocity but, unlike in model M1 (Figure 6), no dominant rotational symmetry (axis) can be observed. This is a clear indication that the anisotropy symmetry is lower than TOR, which was also the final interpretation before model M2 was revealed.

Model M2 revealed (post-inversion)

Model M2 is a triclinic model estimated from real data by Grechka and Yaskevich (2014) corresponding to Middle Bakken siltstone. The anisotropy of the model is moderate ($\sim 10\%$). The model is somewhat troublesome because, to a large degree, it locally violates the assumption behind equation (1), i.e., the ray velocity vector being close to the phase velocity vector both in its size and its direction. Along the vertical, this assumption is significantly violated in M2. See Appendix C for elastic parameters in the Voigt notation used to generate M2 data using elastic finite differences.

To evaluate the inversion accuracy, true A-parameters from the upper part of Table 2 are used in equation (1), and corresponding traveltimes are added to Figure 7 as circles. As predicted, the overall misfit seems slightly worse than in the model M1. The best estimated parameters are now ϵ_x, ϵ_z, all χ parameters and ξ_{15} and ξ_{35}. As in the model M1, and as predicted from the inversion, somewhat worse estimates are obtained for parameters ϵ_y, ξ_{24}, ξ_{16} and ξ_{26}. Finally, the inversion practically failed to recover correct values of η parameters. However, the interesting fact about the inversion is, once again, revealed from the phase-velocity-surfaces in Figure 8. Despite the (sometimes large) misfits of estimated and true A-parameters, the approximately reconstructed phase-velocity surface in the left plot of Figure 8 fits the surface based on the true A-parameters in the right plot of Figure 8 remarkably well. That is, the surfaces are nearly identical over the propagation directions sampled by the VSP experiment. In turn, phase-velocity function (1) reconstructed from the estimated A-parameters in Figure 7, Table 2, reproduces accurately kinematics of this VSP experiment and thus should be well-suited for any migration of the corresponding VSP data. This is potentially significant.

Model M2 examined (post-inversion)

Despite the successful reconstruction of the phase-velocity surface in Figure 8, the failure to invert especially η parameters was troublesome to us. In order to better understand the reasons, and in order to further test the stability of the inversion, we designed a series of additional tests (the tests were no longer blind as model M2 was already revealed at this point). First, we inverted noise-free data. Except for an improvement in the estimate of parameters ξ_{16} and ξ_{26}, we recovered effectively identical set of values as those from the noisy data. Reversely, as the next test we contaminated the data with the noise 2.5x stronger than the original noise level. Resulting data contamination displayed in Figure 9 for the borehole receiver at depth $z = 4000$ m shows noticeably worse S/N compared to the original noise level in Figure 2.

This drop in S/N introduced challenges in traveltime picking, especially at large hypocentral distances, compare Figure 10 with 3. Corresponding inversion results are shown in Figure 11. The increased noise level lead to the increased number of outliers

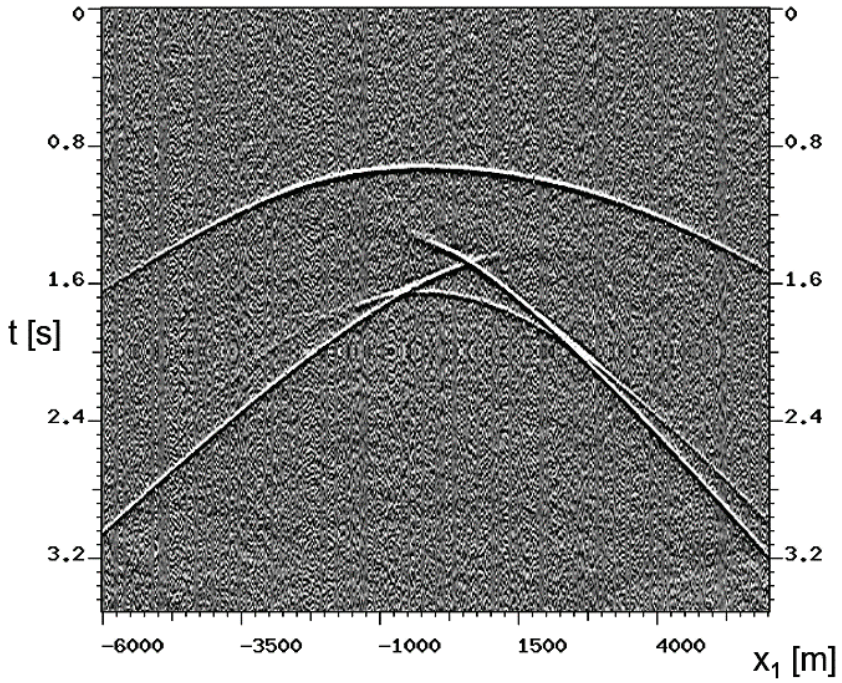

Figure 9: Cross-section of synthetic VSP receiver gather generated for model M2, borehole receiver $x_3 = 4000$ m, in analogy to Figure 2. The data is contaminated by real noise 2.5 $\times$ stronger than that in Figure 2.

in the data. Let us emphasize that the large outliers in the experiment with 2.5x stronger noise weren't removed from the data prior the inversion. Despite of it, the results presented in Figure 11 show slightly better fit with the true data than in Figure 7 for some parameters (specifically for χ_x, χ_z and ξ_{26}). Generally, however, the effect of noise is visible only via the sizes of the estimated error bars, compare Figure 11 with Figure 7.

We also modified the source configuration. We split the data from the complete set of sources into even and odd subsets and inverted them separately (including standard noise). The results differed negligibly from the results shown in Figure 7. When we reorganized sources into a symmetric fan of profiles around the borehole, the result, again, did not change significantly. We thus concluded that, within reasonable limits, the inversion is generally quite robust with respect to both the noise level and the number of sources (source configuration) as long as the source distribution approximately spans the same angles and azimuths.

A significant improvement in the fit of estimated and true parameters occurred, however, when we modified the distribution of receivers in the borehole. Instead of 5 receivers regularly distributed between depths of 4 km and 5 km, we considered 5 receivers regularly distributed between 1 km and 5 km. That effectively means we significantly expanded angular data coverage. Recorded data from shallower receivers sampled the propagation directions up to, approximately, 80° from vertical (as opposed to approximately 55° previously). The downside of adding the shallow receivers was that the traveltime picking from the receivers at 1 km, 2 km, and 3 km depths became more involved. For those

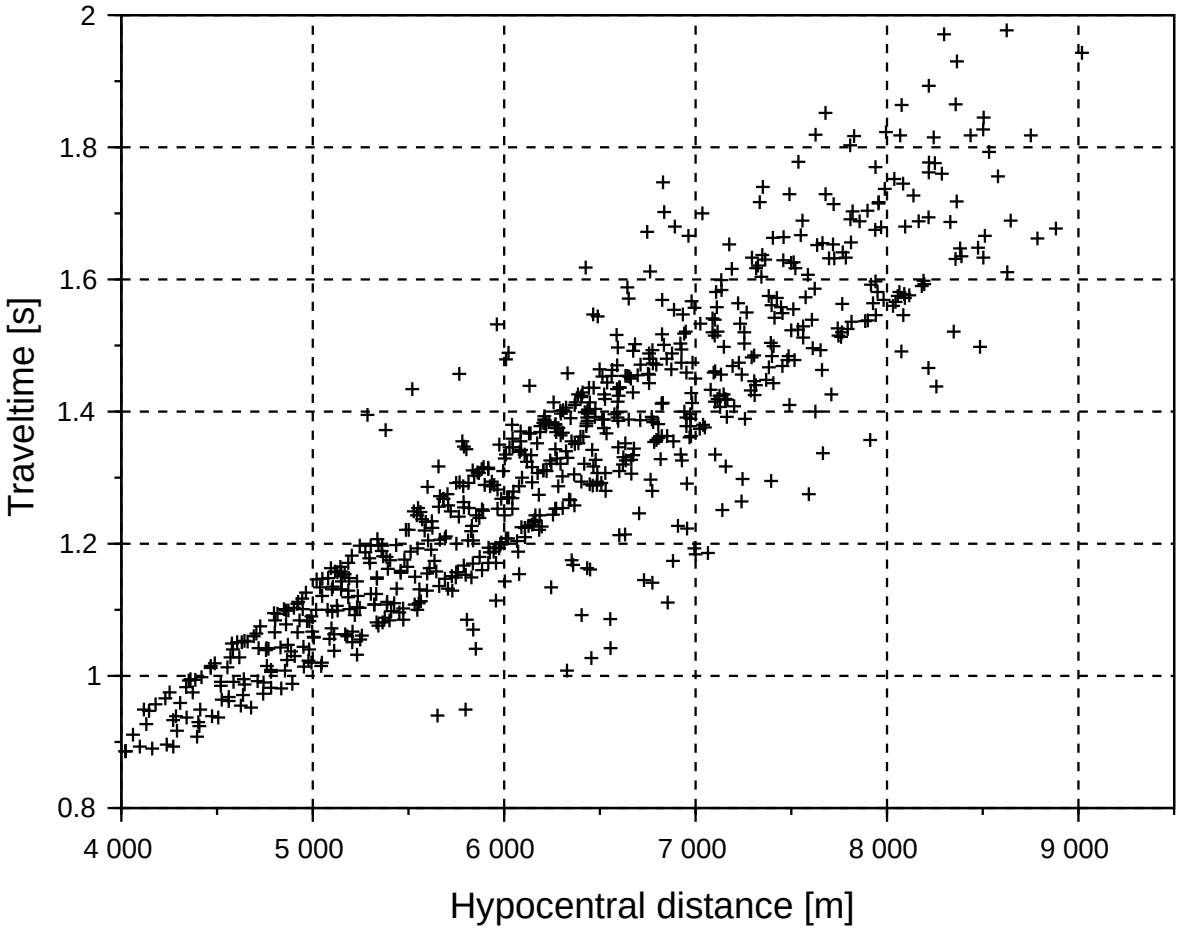

Figure 10: The picked traveltimes plotted against the hypocentral distance of all borehole receivers from surface shots, in analogy to Figure 3. The data is contaminated by real noise 2.5× stronger than that in Figure 3.

depths, the recorded energy propagated in a wide range of angles from near-vertical to close-to-horizontal directions. Therefore, all three x_1, x_2, x_3 receiver components were necessary to capture the energy. Also, for some offsets and azimuths, the P- and S-wave arrivals were close to each other, hence interfering. The traveltime picking thus involved picking on all three components, also accounting for sign changes present on horizontal components, followed by smoothing/filtering of the picked traveltimes. Resulting traveltime picks for receivers at 1 km, 2 km, and 3 km were generally noisier and perhaps more biased (true onset traveltime was not estimated very accurately) than those from deeper receivers at 4 km and 5 km, which was our concern. Results of the inversion are shown in Figure 12. We can see overall improvement in the estimated parameters. A significant improvement can be seen especially for ϵ_y, η_x, η_z, ξ_{16} and ξ_{26} parameters. Figure 13 shows phase-velocity surfaces calculated from equation (1) using estimated (left) and true (right) P-wave A-parameters. The surfaces are very close to each other for all directions now

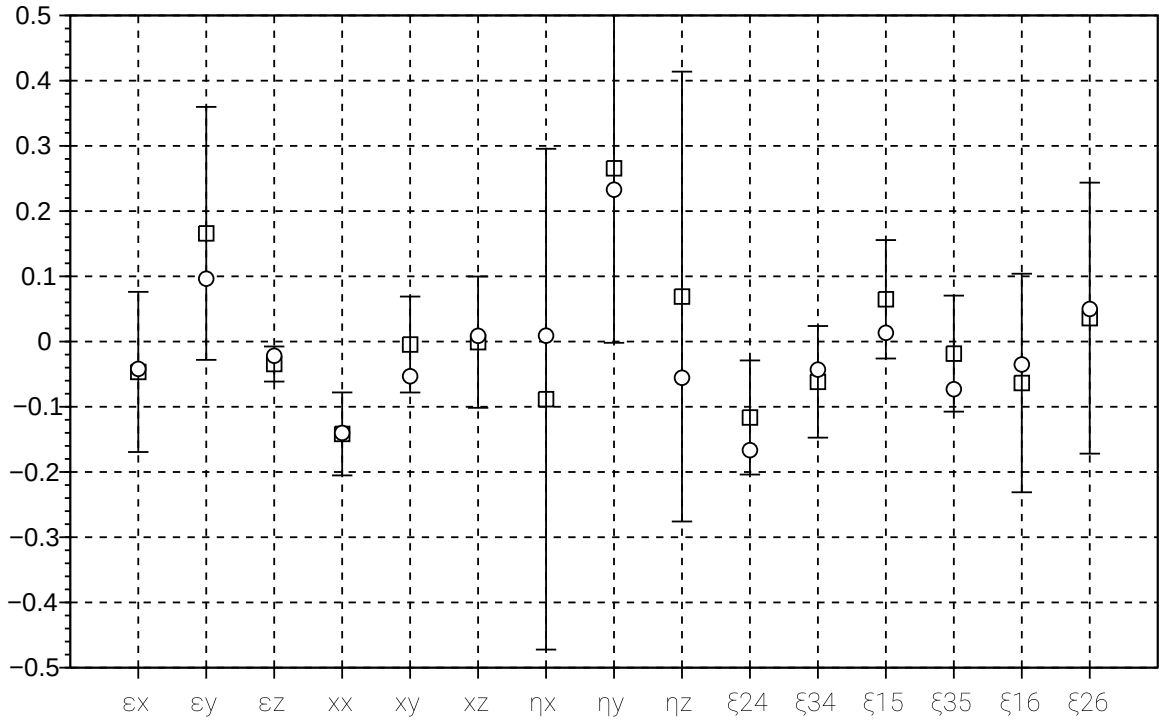

Figure 11: Results of the inversion of traveltime data generated in the model M2 with 2.5 larger realistic noise added to 5 receivers distributed regularly between depths of 4 and 5 km. True (circles) and estimated (squares) A-parameters. Demarcated lines: error bars. Reference velocity used: $\alpha = 4.65$ km/s.

(compare with Figure 8). In such a case, the recovered phase-velocity function could be used in migration of data sets of any configuration (not only the specific VSP configuration used for the inversion) because it is accurately recovered for most angles and azimuths relevant for migration.

From the above experiments, we conclude that a decisive factor for the successful inversion is, not surprisingly, the degree of the angular illumination of the studied subsurface. The phase-velocity function (1) is, however, relatively robust; it can be reconstructed with a good accuracy for a given experiment (i.e., for directions of propagation captured by the experiment) even if some A-parameters are not well-recovered. If the angular illumination is favorable (not necessarily perfect), the velocity function may be recoverable in full. We also conclude from the above experiments that noise and distribution of sources on the surface play secondary roles (within reasonable limits, of course), i.e., problems due to these factors can be largely mitigated during real data acquisition.

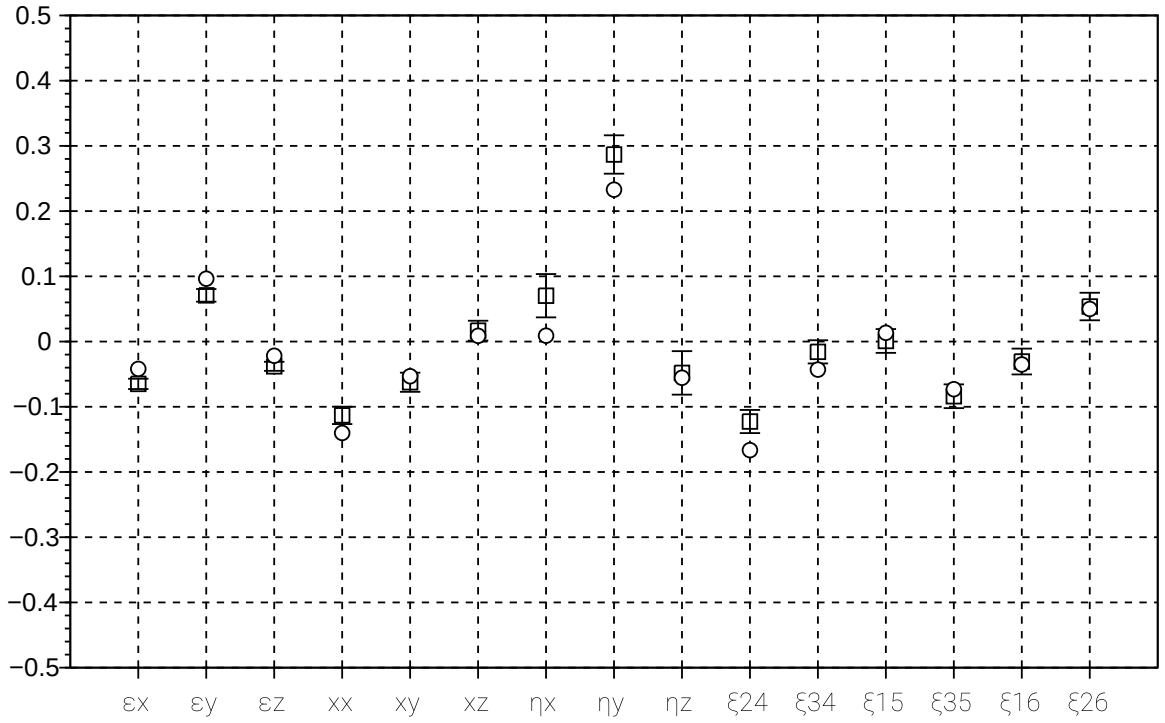

Figure 12: Results of the inversion of traveltime data generated in the model M2 with realistic noise added to 5 receivers distributed regularly between depths of 1 and 5 km. True (circles) and estimated (squares) A-parameters. Demarcated lines: error bars. Reference velocity used: $\alpha = 4.65$ km/s.

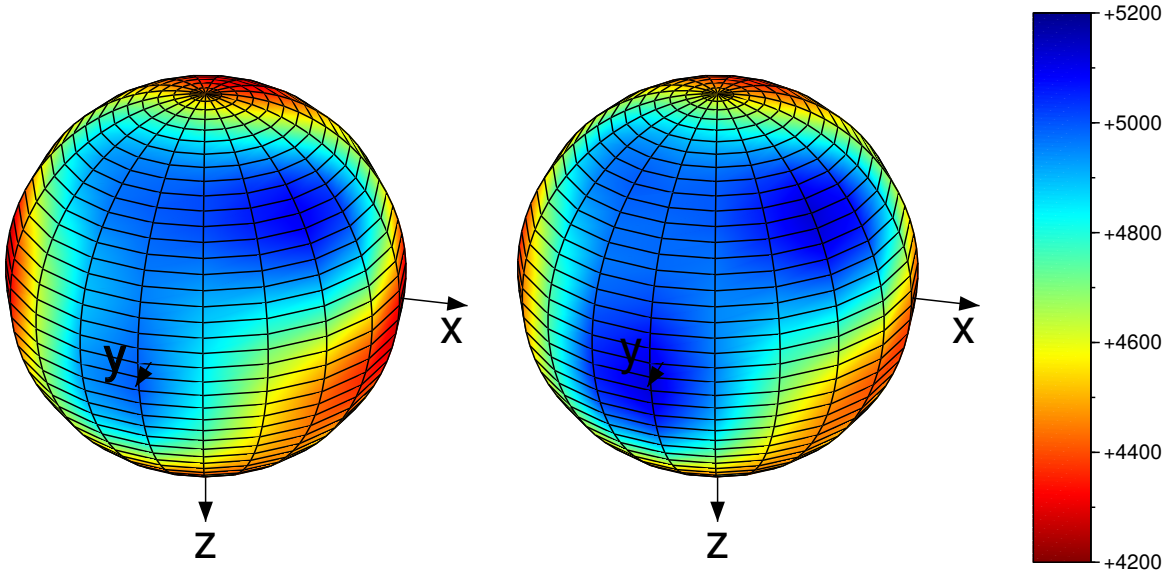

Figure 13: P-wave velocity surfaces calculated from equation (1) for model M2 for 5 receivers distributed regularly between depths of 1 and 5 km. A-parameters estimated from traveltime data and shown in Figure 12 (left), true A-parameters (right) used in equation (1).

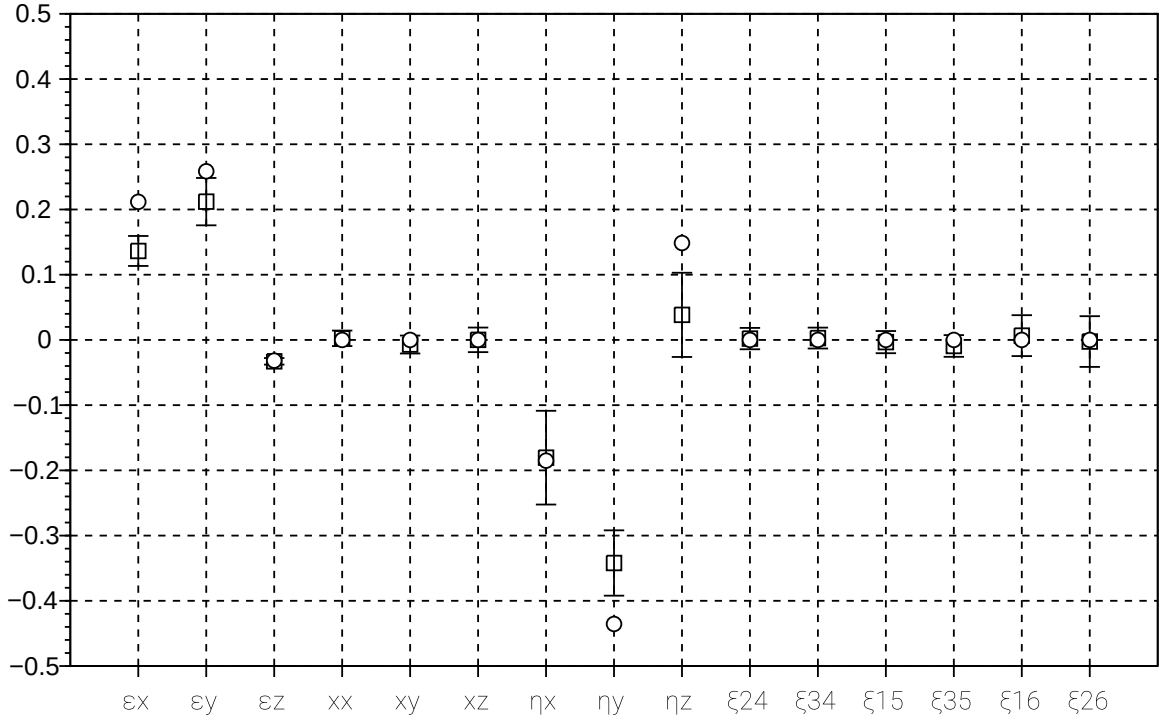

Figure 14: Results of the inversion of traveltime data generated in the model M3 with realistic noise added to 5 receivers distributed regularly between depths of 4 and 5 km. True (circles) and estimated (squares) A-parameters. Demarcated lines: error bars. Reference velocity used: $\alpha = 3.1$ km/s.

Model M3

The final test presented here (model M3) was carried out following the same data processing and inversion flows as described for models M1 and M2 above. The noise contamination was the same as in M1.

Results of the inversion are shown in Figure 14. Squares show again the recovered A-parameters with estimated 3-σ error bars. A distinct feature is immediately observed: recovered parameters χ and ξ are close-to-zero. This strongly suggests VTI or ORT anisotropy (with horizontal symmetry plane coincinding with the (x_1, x_2) plane), for which the only non-zero parameters are ϵ_x, ϵ_y, ϵ_z, η_x, η_y and η_z. Additionally, if the model was VTI, the following would also hold: $\epsilon_x = \epsilon_y$, $\eta_x = \eta_y$, and $\eta_z = 0$. Therefore, we can conclude with a high probability that model M3 is orthorhombic (ORT). The high-degree of symmetry, with one symmetry plane being likely horizontal (ORTH), is also confirmed visually from the displayed phase-velocity surface, see the left plot in Figure 15.

The error bars in Figure 14 suggest high accuracy of the estimates. However, the recovered magnitudes of ϵ_x, ϵ_y, ϵ_z, but also η_x, η_y, η_z also suggest potentially strong anisotropy. As discussed above, error bars do not include errors due to weak-anisotropy assumption, under which the entire inversion scheme operates. Therefore, they only indicate that the A-parameters should be resolved reasonably well with the existing data coverage. However, the error bars are not to be interpreted as reliable estimates of absolute errors in the case of M3.

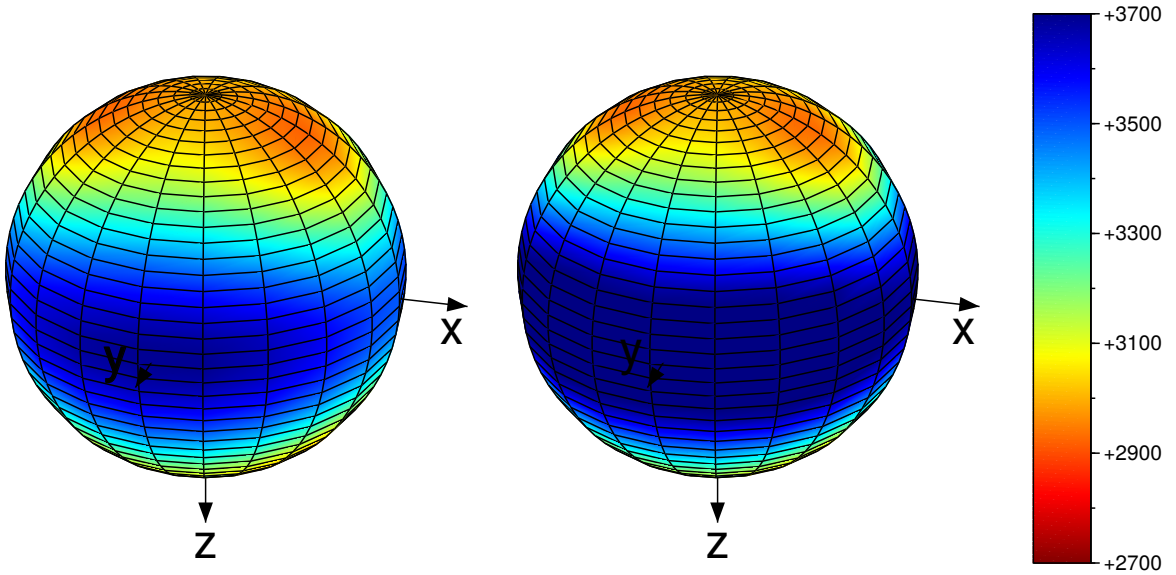

Figure 15: P-wave velocity surfaces calculated from equation (1) for model M3 for 5 receivers distributed regularly between depths of 4 and 5 km. A-parameters estimated from traveltime data and shown in Figure 14 (left), true A-parameters (right) used in equation (1).

Model M3 revealed (post-inversion)

Model M3 was generated to test the limits of the inversion, which were not approached in the previous two experiments. First, the inversion utilizing the anisotropy concept introduced here should be capable of recognizing reliably higher anisotropy symmetries (aligned with coordinate system) by correctly reducing the number of estimated non-zero A-parameters. Second, the inversion should start experiencing problems with increasing anisotropy strength. With that on mind, orthorhombic model M3 was introduced with no rotation applied (i.e., ORTH). Additionally, the model was strongly anisotropic with more than 25% anisotropy, see the values of ϵ_x and ϵ_y in the upper part of Table 3 and the pronounced velocity changes near horizontal and vertical symmetry planes in Figure 15. See also equation (C4) in Appendix C for M3 elastic parameters in the Voigt notation.

The true M3 values of A-parameters from the top of Table 3 are also added to Figure 14 as circles for direct comparison with their estimated counterparts. By-now-familiar

Model M3 A parameters	ϵ_x η_z	ϵ_y ξ_{24}	ϵ_z ξ_{34}	χ_x ξ_{15}	χ_y ξ_{35}	χ_z ξ_{16}	η_x ξ_{26}	η_y
true	0.2118 0.1485	0.2586 0.	-0.0317 0.	0. 0.	0. 0.	0. 0.	-0.1852 0.	-0.4356
estimated	0.1364 0.0385	0.2120 0.0020	-0.0328 0.0028	0.0024 -0.0033	-0.0070 -0.0092	0.0001 0.0066	-0.1816 -0.0025	-0.3420

Table 3: 15 true and estimated P-wave A-parameters of the model M3. P-wave reference velocity chosen $\alpha = 3.1$ km/s.

misfits of η_y and η_z parameters can be quickly recognized. As we know from the M2 experiments above, the misfits would improve if a better illumination was available (as, for example, the one in Figure 12). The presence of misfits of ϵ_x and ϵ_y parameters is an obvious consequence of the strength of M3 anisotropy. On the other hand, the parameters χ_x, χ_y, χ_z, ξ_{24}, ξ_{34}, ξ_{15}, ξ_{35}, ξ_{16} and ξ_{26}, which are zero for ORTH model M3, are estimated very well. Finally, and in agreement with all the previous inversions, despite the distortions observed in A-parameters, Figure 15 offers nearly perfect fit of phase-velocity surfaces calculated from equation (1) using estimated (left) and true (right) A-parameters, even in this strongly anisotropic ORTH model.

In conclusion, the inversion of M3 succeeded in recognizing higher anisotropy symmetry despite a clear violation of the weak-anisotropy assumption. It also correctly indicated stronger anisotropy. Because of the strong anisotropy, the actual A-parameters corresponding to ORTH symmetry were recovered with a lower accuracy (hence not well-suited for rock property interpretation, for example). However, the phase-velocity surface reconstructed using those parameters (i.e., without any a priori knowledge of the anisotropy symmetry) is nearly identical to that calculated using the true A-parameters. Therefore, such a velocity should be adequate for migration even in media with stronger anisotropy, or as a starting velocity model for anisotropic FWI.

Conclusions

An alternative, practical approach to seismic anisotropy, in which a set of anisotropy parameters is sought without a priori information about the anisotropy symmetry and its orientation, is proposed. The inversion scheme resulting from this approach is based on the use of the first-order weak-anisotropy approximation of the ray (group) velocity, which is expressed in terms of 15 P-wave A-parameters. The use of these two concepts (A-parameters and the first-order weak-anisotropy approximation) offers a simple physical insight and simplifies the underlying theory. The separation of P-wave expressions from those for S waves is natural. No non-physical assumptions, such as the pseudo-acoustic assumption (phase S-wave velocity set to zero for a specified direction), are needed. We suggest that these properties make the implementation of arbitrary anisotropy in seismic data processing practical. That includes inversion for A-parameters that are clearly linked to various seismic attributes and thus, in principle, extractable from measurements. With the use of estimated A-parameters, we can reconstruct various seismic attributes, such as phase velocity, to a high degree of accuracy. Phase-velocity function then can be directly used, for example, in migrations, modeling, or FWI. No in-between interpretation steps are required.

We applied the above concept in a blind inversion of synthetic VSP data for P-wave A-parameters. We chose synthetic data to ultimately maintain the control as this was our first inversion of this kind. However, the data was generated independently from the inversion using BP elastic FD modeling, then contaminated by real VSP noise. P-wave traveltimes were picked using industry-standard picking software. The inversion was performed completely separately and without any knowledge of anisotropy symmetry and strength. We tested the inversion for three different symmetries and different anisotropy strengths, concluding the following:

a) within reasonable limits, the inversion is robust in terms of noise level and a source-receiver distribution pattern used (assuming similar angle span across different patterns);

b) the most important factor is angular data coverage (sampling various propagation angles);

c) the inversion can naturally recognize higher anisotropy symmetry with symmetry elements coinciding with coordinate planes or lines, and contracts the set of A-parameters accordingly (by estimating relevant A-parameters as close-to-zero);

d) phase-velocity surface can be reconstructed from the estimated A-parameters (even if not fully resolved), and anisotropy can be further interpreted for symmetry type and orientation;

e) for stronger anisotropy (above 25%), estimation of A-parameters is less accurate, but phase-velocity surface can still be reconstructed with a high degree of accuracy.

We therefore conclude that using the proposed concept we can reconstruct a phase-velocity function that should be directly applicable in migration or as a starting model for FWI, if desired, without a priori knowledge (or interpretation) of anisotropy symmetry and its orientation. The concept should be applicable for many real-world scenarios where the effective anisotropy of the subsurface is known to vary from weak to moderate in strength.

In terms of implementation, due to well-defined relations of A-parameters to more conventional parameters used in industry today (Thomsen, 1986; Tsvankin, 1997), many computer codes and processing tools designed for higher anisotropy symmetries can be extended to herein discussed arbitrary anisotropy by, in principle, a relatively simple alterations of their kernels. That includes dispersion relations used in various migration or modeling codes.

Finally, as the type and orientation of anisotropy does not need to be a priori known, we suggest that the herein proposed concept should be well-suited for practical data processing not only in low-symmetry anisotropic subsurface but also in subsurface with simpler but tilted anisotropy symmetry (TTI, TOR), or subsurface with anisotropy symmetry spatially variable or otherwise unknown.

Acknowledgements

We are grateful to BP America Inc., Subsurface Technology Center, Houston, USA, the Research Project 16-05237S of the Grant Agency of the Czech Republic, and the project "Seismic waves in complex 3-D structures" (SW3D) for support.

Appendix A: Inversion scheme

We start with equation (2):

$$\mathbf{G}\mathbf{m} = \mathbf{d}. \tag{A1}$$

$\mathbf{G}$ represents the $N \times M$ forward operator matrix, N is the number of observations and M is the number of sought A-parameters. In our case $M = 15$. The rows of matrix $\mathbf{G}$ have the following form:

$$\begin{aligned}(&N_1^2 \quad N_2^2 \quad N_3^2 \quad 2N_2N_3 \quad 2N_1N_3 \quad 2N_1N_2 \quad N_2^2N_3^2 \quad N_1^2N_3^2 \quad N_1^2N_2^2 \\ &-2N_2^3N_3 \quad -2N_3^3N_2 \quad -2N_1^3N_3 \quad -2N_1N_3^3 \quad -2N_1^3N_2 \quad -2N_1N_2^3)\ .\end{aligned} \tag{A2}$$

Here, the individual elements are formed from components of the ray vector $\mathbf{N}$:

$$\mathbf{N} \equiv (N_1, N_2, N_3)^T\ . \tag{A3}$$

The symbol T indicates transposition. Each row in matrix $\mathbf{G}$ corresponds to one particular ray (connecting one source and one receiver). Symbol $\mathbf{m}$ in (A1) denotes the vector of model parameters to be determined. In our case, it consists of 15 P-wave A parameters m_i ordered as:

$$\mathbf{m} \equiv (\epsilon_x, \epsilon_y, \epsilon_z, \chi_x, \chi_y, \chi_z, \eta_x, \eta_y, \eta_z, \xi_{24}, \xi_{34}, \xi_{15}, \xi_{35}, \xi_{16}, \xi_{26})^T. \tag{A4}$$

Vector $\mathbf{d}$ in (A1) has the following form:

$$\mathbf{d} \equiv \frac{1}{2}\Big((\frac{r_1}{\alpha_0 t_1})^2 - 1,\ (\frac{r_2}{\alpha_0 t_2})^2 - 1,\ ....,\ (\frac{r_N}{\alpha_0 t_N})^2 - 1\Big)^T\ , \tag{A5}$$

where symbols r_i denote source-receiver distances corresponding to traveltimes t_i. Squared traveltimes t_i, $i = 1, ..., N$ appear in the denominator. Note that the relation between traveltimes and A parameters is nonlinear.

Using all available data, equation (A1) can be solved by pseudoinverse (e.g., Aster et al., 2013; Press et al., 2007):

$$\mathbf{m} = \mathbf{G}^\dagger\mathbf{d}. \tag{A6}$$

Here, $\mathbf{G}^\dagger$ denotes the pseudoinverse of matrix $\mathbf{G}$. Note that the pseudoinverse automatically provides least square solution for an overdetermined problem and least-norm solution for an underdetermined problem.

An important part of the inversion is the assesment of errors of estimated A-parameters. The simplest way how to asses their errors is to transform the data covariance matrix $\mathbf{C}_d$ to the model covariance matrix $\mathbf{C}_m$:

$$\mathbf{C}_m = \mathbf{G}^{\dagger T}\mathbf{C}_d\mathbf{G}^\dagger. \tag{A7}$$

Since we do not know the data covariance matrix $\mathbf{C}_d$ exactly, we must use its approximation. We choose $\mathbf{C}_d$ as follows:

$$\mathbf{C}_d \approx \sigma^2\mathbf{I}. \tag{A8}$$

Here $\mathbf{I}$ is 15×15 identity matrix. The value of the parameter σ can be determined using χ^2 statistics of residuals $\mathbf{r} = \mathbf{d} - \mathbf{G}\mathbf{m}$ with number of degree of freedom $\nu = N - M$: since we have

$$\nu^{-1}\mathbf{r}^T\mathbf{C}_d^{-1}\mathbf{r} = \nu^{-1}\sigma^{-2}\mathbf{r}^T\mathbf{r} \approx 1, \tag{A9}$$

we get

$$\sigma = \sqrt{\nu^{-1}\mathbf{r}^T\mathbf{r}}. \qquad (A10)$$

Using equation (A7), we can thus estimate the model covariance matrix $\mathbf{C}_m$. Square roots of diagonal elements of $\mathbf{C}_m$ then represent Gaussian errors of individual A-parameters.

Appendix B

P-wave A-parameters

The P-wave A-parameters are defined as follows, see, e.g., Pšenčík et al. (2018):

$$\epsilon_x = \frac{A_{11}-\alpha^2}{2\alpha^2}\ , \quad \epsilon_y = \frac{A_{22}-\alpha^2}{2\alpha^2}\ , \quad \epsilon_z = \frac{A_{33}-\alpha^2}{2\alpha^2}\ ,$$

$$\chi_x = \frac{A_{14}+2A_{56}}{\alpha^2}, \quad \chi_y = \frac{A_{25}+2A_{46}}{\alpha^2}, \quad \chi_z = \frac{A_{36}+2A_{45}}{\alpha^2},$$

$$\eta_x = \frac{2(A_{23}+2A_{44})-A_{22}-A_{33}}{2\alpha^2}, \quad \eta_y = \frac{2(A_{13}+2A_{55})-A_{33}-A_{11}}{2\alpha^2},$$

$$\eta_z = \frac{2(A_{12}+2A_{66})-A_{11}-A_{22}}{2\alpha^2},$$

$$\xi_{24} = \frac{A_{14}+2A_{56}-A_{24}}{\alpha^2}, \quad \xi_{34} = \frac{A_{14}+2A_{56}-A_{34}}{\alpha^2}, \quad \xi_{15} = \frac{A_{25}+2A_{46}-A_{15}}{\alpha^2},$$

$$\xi_{35} = \frac{A_{25}+2A_{46}-A_{35}}{\alpha^2}, \quad \xi_{16} = \frac{A_{36}+2A_{45}-A_{16}}{\alpha^2}, \quad \xi_{26} = \frac{A_{36}+2A_{45}-A_{26}}{\alpha^2}\ . \qquad (B1)$$

The symbol α is a P-wave velocity in a reference isotropic medium. The symbols $A_{\alpha\beta}$ denote the elements of the 6×6 matrix of the density-normalized elastic parameters in the Voigt notation.

Appendix C

Elastic parameters of M1, M2, and M3 models used in the inversion experiments

Model "M1" discussed in the main text is a TOR model of a moderate anisotropy strength. In the coordinate system aligned with the orthorhombic symmetry planes, the corresponding matrix of the density-normalized elastic parameters in $(\mathrm{km/s})^2$ reads:

$$\begin{pmatrix} 12.959 & 3.000 & 3.364 & 0.000 & 0.000 & 0.000 \\ & 13.721 & 2.597 & 0.000 & 0.000 & 0.000 \\ & & 10.890 & 0.000 & 0.000 & 0.000 \\ & & & 4.483 & 0.000 & 0.000 \\ & & & & 4.000 & 0.000 \\ & & & & & 5.200 \end{pmatrix}. \qquad (C1)$$

The matrix (C1) was rotated in the manner described in the text to obtain M1 TOR model with the TOR matrix:

$$\begin{pmatrix} 12.807 & 3.031 & 3.331 & -0.149 & -0.297 & 0.251 \\ & 12.958 & 2.867 & 0.695 & -0.089 & 0.231 \\ & & 11.271 & 0.379 & -0.150 & -0.216 \\ & & & 4.709 & 0.070 & -0.049 \\ & & & & 4.272 & 0.398 \\ & & & & & 4.969 \end{pmatrix}. \qquad (C2)$$

The A-parameters corresponding to the rotated matrix (C2), for which the "observed" traveltimes are generated, are given in Table 1.

Model "M2" from the main text represents Middle Baker siltstone of triclinic anisotropy symmetry and moderate anisotropy strength (see Grechka and Yaskevich, 2014). Its matrix of density-normalized elastic parameters reads:

$$\begin{pmatrix} 19.810 & 8.620 & 9.000 & -2.370 & -1.440 & 0.950 \\ & 25.790 & 9.090 & 0.570 & -0.990 & -0.890 \\ & & 20.680 & -2.100 & 0.430 & 0.490 \\ & & & 7.170 & -0.150 & -0.080 \\ & & & & 8.140 & -0.330 \\ & & & & & 6.490 \end{pmatrix}. \qquad (C3)$$

The corresponding A-parameters are given in Table 2.

Model "M3" is a strongly anisotropic model of orthorhombic symmetry with the matrix of density-normalized elastic parameters as follows:

$$\begin{pmatrix} 13.680 & 11.198 & 4.275 & 0.000 & 0.000 & 0.000 \\ & 14.580 & 6.839 & 0.000 & 0.000 & 0.000 \\ & & 9.000 & 0.000 & 0.000 & 0.000 \\ & & & 1.586 & 0.000 & 0.000 \\ & & & & 1.440 & 0.000 \\ & & & & & 2.180 \end{pmatrix}. \qquad (C4)$$

The corresponding A-parameters are given in Table 3.

References

Alkhalifah, T., 1998. Acoustic approximations for processing in transversely isotropic media: Geophysics, **63**, 623–631.

Alkhalifah, T., 2000. An acoustic wave equation for anisotropic media: Geophysics, **65**, 1239–1250.

Alkhalifah, T., and P. Sava, 2010. A transversely isotropic medium with a tilted symmetry axis normal to the reflector: Geophysics, **75**, A19–A24.

Arts, R. J., 1993. A study of general anisotropic elasticity in rocks by wave propagation: Theoretical and experimental aspects: Ph.D. thesis, Institut Français du Pétrole.

Aster, R. C., B. Borchers, and C. H. Thurber, 2013. Parameter estimation and inverse problems: Academic Press, Oxford.

Audebert F., V. Dirks, and A. Pettenati, 2006. TTI anisotropic depth migration: What tilt estimate should we use?: SEG, Expanded Abstracts, 2382–2386.

Bai, C-Y, T. Wang, S-B. Yang, X-W. Li, and G-J. Huang, 2016. Simultaneous elastic parameter inversion in 2-D/3-D TTI medium combined later arrival times: Journal of Seismology, **20**, 475–494.

Bakulin, A., M. Woodward, D. Nichols, K. Osypov, and O. Zdraveva, 2009. Building TTI depth models using anisotropic tomography with well information: SEG, Expanded Abstracts, 4029–4033.

Behera, L., and I. Tsvankin, 2007. Migration velocity analysis and imaging for tilted TI media: SEG, Expanded Abstracts, 129–133.

Billette, F. J., and S. Brandsberg-Dhal, 2005. The 2004 BP velocity benchmark: the 67th Conference and Exhibition, EAGE, Expanded Abstracts, B035.

Červený, V., 1989. Ray tracing in factorized anisotropic inhomogeneous media: Geophysical Journal International, **99**, 91-100.

Chapman, C.H., and R. G. Pratt, 1992. Traveltime tomography in anisotropic media - I. Theory: Geophysical Journal International, **109**, 1–19.

Chu, C., B. K. Macy, and P. D. Anno, 2011. Approximation of pure acoustic seismic wave propagation in TTI media: Geophysics, **76**, WB97-WB107.

Chu, C., B. K. Macy, and P. D. Anno, 2013. Pure acoustic wave propagation in transversely isotropic media by the pseudospectral method: Geophysical Prospecting, **61**, 556-567.

Dellinger, J., J. R. Sandschaper, C. Regone, J. Etgen, and I. Ahmed, 2015. The Garden Banks Model Experience: SEG, Expanded Abstracts, 5202–5206.

Duveneck, E., P. Milcik, P. M. Bakker, and C. Perkins, 2008. Acoustic VTI wave equations and their application for anisotropic reverse-time migration: SEG, Expanded Abstracts, 2186-2190.

Etgen, J. T., and S. Brandsberg-Dahl, 2009. The pseudo-analytical method: application of pseudo-Laplacians to acoustic and acoustic anisotropic wave propagation: SEG, Expanded Abstracts, 2552-2556.

Farra, V., and I. Pšenčík, 2003. Properties of the zero-, first- and higher-order approximations of attributes of elastic waves in weakly anisotropic media: Journal of Acoustical Society of America, **114**, 1366–1378.

Farra, V., and I. Pšenčík, 2016. Weak-anisotropy approximations of P-wave phase and ray velocities for anisotropy of arbitrary symmetry: Studia geophysica et geodaetica, **60**, 403–418.

Farra, V., and I. Pšenčík, 2017. Weak-anisotropy moveout approximations for P waves in homogeneous TOR layers: Geophysics, **82**, WA23-WA32.

Farra, V., I. Pšenčík, and P. Jílek, 2016. Weak-anisotropy moveout approximations for P waves in homogeneous layers of monoclinic or higher anisotropy symmetries: Geophysics, **81**, C39-C59.

Fedorov, F. I., 1968. Theory of elastic waves in crystals: Plenum Press.

Fowler, P. J., X. Du, and R. P. Fletcher, 2010. Coupled equations for reverse time migration in transversely isotropic media: Geophysics, **75**, S11–S22.

Fowler, P. J., and R. King, 2011. Modeling and reverse time migration of orthorhombic pseudo-acoustic P-waves: SEG, Expanded Abstracts, 190–195.

Grechka, V., and S. Yaskevich, 2014. Azimuthal anisotropy in microseismic monitoring: A Bakken case study: Geophysics, **79**, KS1–KS12.

Hirahara, K., and Y. Ishikawa, 1984. Travel time inversion for three-dimensional P-wave velocity anisotropy: J. Phys. Earth, **32**, 197–218.

Huang, T., S. Xu, J. Wang, and G. Ionescu, 2008. The benefit of TTI for dual-azimuth data in Gulf of Mexico: SEG, Expanded Abstracts, 1, 222-226.

Jech, J., 1991. Computation of elastic parameters of anisotropic medium from traveltimes of quasi-compressional waves: Physics of the Earth and Planetary Interiors, **66**, 153–159.

Jech, J., and I. Pšenčík, 1992. Kinematic inversion for qP and qS waves in inhomogeneous anisotropic structures: Geophysical Journal International, **108**, 604–612. Erratum, 1992. Geophysical Journal International, **110**, 397.

Jin, H., I. Ahmed, J. Mika, C. Kanu, K. Vincent, P. Paramo, B. Nolte, and X. Shen, 2018. Azimuthally sectored TTI FWI and imaging for orthorhombic data using OBN data: A case study from offshore Trinidad: SEG, Expanded Abstracts, 1103–1107.

Kumar, D., M. K. Sen, and R. J. Ferguson, 2004. Traveltime calculation and prestack depth migration in tilted transversely isotropic media: Geophysics, **69**, 37–44.

Li, Y., W. Han, C. Chen, and T. Huang, 2012. Velocity model building for tilted orthorhombic depth imaging: SEG, Expanded Abstracts: 1–5.

Li, X., and H. Zhu, 2018. A finite-difference approach for solving pure quasi-P-wave equations in transversely isotropic and orthorhombic media: Geophysics, **83**, C161–C172.

Mahmoudian, F., G. F. Margrave, P. F. Daley, J. Wong, and D. C. Henley, 2014. Estimation of elastic stiffness coefficients of an orthorhombic physical model using group velocity analysis on transmission data: Geophysics, **79**, R27-R39.

Mathewson, J., R. Bachrach, M. Ortin, M. Decker, S. Kainkaryam, A. Cegna, P. Paramo, K. Vincent, and J. Kommedal, 2015. Offshore Trinidad tilted orthorhombic imaging of full-azimuth OBC data: SEG, Expanded Abstracts 2015: 356–360.

Mensch, T., and V. Farra, 2002. P-wave tomography in inhomogeneous orthorhombic media. Pure and applied geophysics, **159**, 1855-1879.

Mensch, T., and P. Rasolofosaon, 1997, Elastic-wave velocities in anisotropic media of arbitrary symmetry – generalization of Thomsens parameters ϵ, δ and γ: Geophysical Journal International, **128**, 43–64.

Neep, J. P., 2008. Benchmarking Prestack AVO Inversion: 70th EAGE Expanded Abstracts.

Pratt, R. G., and C. H. Chapman, 1992. Traveltime tomography in anisotropic media - II. Application: Geophysical Journal International, **109**, 20–37.

Press, W. H., B. P. Flannery, S. A. Teukolsky, and W. T. Vetterling, 2007. Numerical recipes: Cambridge University Press, Cambridge.

Pšenčík, I., and V. Farra, 2017. Reflection moveout approximations for P-waves in a moderately anisotropic homogeneous tilted transverse isotropy layer: Geophysics, **82**, C175-C185.

Pšenčík, I., and D. Gajewski, 1998. Polarization, phase velocity and NMO velocity of qP waves in arbitrary weakly anisotropic media: Geophysics, **63**, 1754–1766.

Pšenčík, I., B. Růžek, T. Lokajíček, and T. Svitek, 2018. Determination of rocksample anisotropy from P and Swave traveltime inversion: Geophys. J. Int., **214**, 1088-1104.

Reta-Tang, C., W. Conway, H. Xun, and M. Kieling, 2015. Bringing New Clarity to the Campos Basin Using Broadband and TTI Imaging: A Case Study: 14th International Congress of the Brazilian Geophysical Society & EXPOGEF, Rio de Janeiro, Brazil, 3-6 August 2015: 1000–1004.

Rollins F. O., P. O. Ariston, J. Bowling, W. Gou, S. Ji, and Y. Li, 2013. TTI imaging with multi-wide azimuth data - A case study at Mad Dog, GOM: SEG, Expanded Abstracts: 3804–3809.

Růžek, B., and I. Pšenčík, 2016. P-wave VSP traveltime inversion in weakly and moderately anisotropic media: Seismic Waves in Complex 3-D Structures, **26**, 17–59, online at "http://sw3d.cz".

Svitek, T., V. Vavryčuk, T. Lokajíček, and M. Petružálek, 2014. Determination of elastic anisotropy of rocks from P- and S-wave velocities: numerical modelling and lab measurements: Geophysical Journal International, **199**, 1682–1697.

Thomsen, L., 1986. Weak elastic anisotropy: Geophysics, **51**, 1954–1966.

Thanoon, D., R. Bachrach, O. Zdraveva, and S. Chen, 2016. Geomechanics-based tilted orthorhombic modeling workflow for imaging: SEG, Expanded Abstracts, 306–310.

Tsvankin, I., 1997. Anisotropic parameters and P-wave velocity for orthorhombic media: Geophysics, 62, 1292–1309.

Vestrum, R. W., 1994. Group- and phase-velocity inversions for the general anisotropic stiffness tensor: PhD thesis, The University of Calgary.

Vestrum, R. W, D. C. Lawton, and R. Schmid, 1999. Imaging structures below dipping TI media: Geophysics, **64**, 1239–1246.

Watanabe, T., T. Hirai, and K. Sassa, 1996. Seismic traveltime tomography in anisotropic heterogeneous media: J. Appl. Geophys., **35**, 133-143.

Witte, P., F. Herrmann, and C. Stolk, 2016. Phase velocity error minimizing scheme for the anisotropic pure P-wave equation: SEG, Expanded Abstracts, pp. 452–457.

Wu, H., J.M. Lees, 1999. Cartesian parameterization of anisotropic traveltime tomography: Geophysical Journal International, **137**, 64-80.

Wu, Q., Y. Li, and Z. Li, 2013. Improved subsalt imaging of full azimuth data with tilted orthorhombic PSDM: SEG, Expanded Abstracts, 3810–3814.

Zdraveva, O., and M. Cogan, 2011. Building Anisotropic models for large scale TTI imaging in areas with limited well control: Kwanza basin case study: 73rd EAGE Conference and Exhibition, Extended Abstracts.

Zdraveva, O., R. Bloor, and D. Nichols, 2015. Anisotropic depth imaging in presence of stress: Transversely Isotropic or orthorhombic?: ASEGPESA.

Zhan, G., R. C. Pestana, and P. L. Stoffa, 2012. Decoupled equations for reverse time migration in tilted transversely isotropic media: Geophysics, **77**,T37–T45.

Zhou, B., S. Greenhalgh, and A. Green, 2008. Nonlinear traveltime inversion scheme for crosshole seismic tomography in tilted transversely isotropic media: Geophysics, **73**, D17–233.

Zhou, B., J. Zhou, L. Liu, F. C. Loh, J. Liu, Y. Xie, Z. Wang, and X. Pu, 2015. Orthorhombic velocity model building and imaging of Luda field with WAZ OBC data: SEG, Expanded Abstracts, 5212–5216.